

A role for the cortex in sleep-wake regulation

Lukas B. Krone^{1,2}, Tomoko Yamagata^{2,3}, Cristina Blanco-Duque^{1,2,4},
Mathilde C. C. Guillaumin^{2,3,5}, Martin C. Kahn^{1,2,4}, Vincent van der Vinne^{1,2,6},
Laura E. McKillop^{1,2}, Shu K. E. Tam^{2,3}, Stuart N. Peirson^{2,3}, Colin J. Akerman⁷,
Anna Hoerder-Suabedissen¹, Zoltán Molnár^{1*}, Vladyslav V. Vyazovskiy^{1,2*}

Affiliations

¹Department of Physiology, Anatomy and Genetics, University of Oxford, UK

² Sleep and Circadian Neuroscience Institute, University of Oxford, UK

³Nuffield Department of Clinical Neurosciences, University of Oxford, UK

⁴The Picower Institute for Learning and Memory, Massachusetts Institute of Technology, MA,
USA

⁵Institute for Neuroscience, Department of Health Sciences and Technology, ETH Zürich, CH

⁶Department of Biology, Williams College, MA, USA

⁷Department of Pharmacology, University of Oxford, UK

Key words: sleep homeostasis, cortex, layer 5, EEG, slow-wave activity, sleep, SNAP25

*Corresponding authors

Vladyslav V. Vyazovskiy

Department of Physiology, Anatomy and Genetics,

Sleep and Circadian Neuroscience Institute (SCNi),

Dunn School of Pathology, South Parks Road, Oxford, OX1 3RE

Phone: +44 (0) 1865 618676

E-mail: vladyslav.vyazovskiy@dpag.ox.ac.uk

Zoltán Molnár

Department of Physiology, Anatomy and Genetics,

- 32 Sherrington Building, Sherrington Road, Oxford, OX1 3PT
- 33 Phone: +44 (0) 1865 282664
- 34 E-mail: zoltan.molnar@dpag.ox.ac.uk

Abstract

The cortex and subcortical circuitry are thought to play distinct roles in the generation of sleep oscillations and global control of vigilance states. Here we silenced a subset of neocortical layer 5 pyramidal and archicortical dentate gyrus granule cells in mice using a cell-specific ablation of the key t-SNARE protein SNAP25, and investigated the effects of this cortical manipulation on sleep. We found a marked increase in wakefulness accompanied by a reduced rebound of EEG slow-wave activity after sleep deprivation. Our data illustrates an important role for [neurons in neo- and archicortex](#) in global state control and sleep homeostasis.

Main text

The duration, timing and architecture of sleep are strictly regulated. Early studies based on neurological case reports, transections and electrical stimulation suggested that global state transitions are mediated via a distributed circuitry across the brainstem, the hypothalamus and the basal forebrain. More recent studies using selective targeting of specific neuronal populations based on their gene expression or connectivity patterns, highlighted that the sleep-wake promoting circuitry is highly complex, with distinct subcortical brain regions and neuronal subtypes responsible for specific aspects of wakefulness and sleep^{1,2}. Although sleep-wake states are defined by the occurrence of neocortical and hippocampal oscillations, the possibility that **neo- and archicortical neurons** control vigilance states has been overlooked.

Cortical oscillations and neuronal firing patterns mirror sleep homeostasis^{3,4}. Sleep homeostasis refers to the adjustment of the duration and intensity of sleep, to the duration of preceding wakefulness⁴. Electroencephalogram (EEG) slow-wave activity (SWA, EEG spectral power between 0.5-4 Hz) during NREM sleep represents a reliable marker of sleep-wake history⁴ and has been proposed to underlie many functions of sleep, such as cellular maintenance and synaptic plasticity. SWA can be regulated in a local, use-dependent manner^{5,6}, in line with the view that sleep emerges within cortical networks driven by the local accumulation of metabolic products, such as adenosine⁷. However, slow waves also occur under anaesthesia, in isolated cortical slabs or even *ex vivo*⁸. Therefore, the capacity to produce slow waves does not automatically imply a causative role for the cortex in physiological sleep or sleep homeostasis, either on a local or global level.

Here we test whether cortical structures have a function in regulating global sleep-wake dynamics. We focused on pyramidal neurons within layer 5 of the neocortex as well as archicortical dentate gyrus granule cells, two cell types involved in the generation of sleep oscillations. Layer 5 pyramidal neurons have been shown essential for the initiation and propagation of neocortical slow waves^{9–11}, the main type of NREM sleep oscillations. Dentate gyrus granule cells contribute to the generation of hippocampal theta rhythm¹², the defining oscillatory activity of REM sleep in rodents¹³. Yet neither of these two neo- and archicortical cell populations has so far been implicated in sleep-wake control.

Laminar local field potential (LFP) and multiunit activity (MUA) recordings were performed from the primary motor cortex of male adult wild type (C57BL/6) mice, concomitantly with EEG and electromyography (EMG) monitoring during 24 h undisturbed conditions (Figure 1a-e). Consistent with the idea of an active role for layer 5 in generating slow waves^{9,10,14}, we found that neurons in layer 5 tended to initiate spiking upon the onset of population ON periods (Figure 1e, Suppl. Fig 1). A leading role for layer 5 was indicated by a stronger initial surge of neuronal firing at OFF-ON transitions (Suppl. Fig. 1a), and a shorter latency to the first spike during ON periods, even when the total number of spikes in layer 5 was matched with layer 2/3 (Suppl. Fig. 1b).

To induce a cortex-wide reduction in the output from layer 5 pyramidal neurons, we used a transgenic mouse line, in which a subpopulation (~15-30 %) of pyramidal cells in layer 5 of the neocortex lack the key t-SNARE protein SNAP25 (Rbp4-Cre;Ai14;Snap25^{fl/fl})¹⁵. Rbp4-Cre is known as a pan layer 5 driver line (Figure 1f, Suppl. Figure 2)¹⁶, but also presents a strong Cre-expression in dentate gyrus granule cells (Suppl. Figure 3). By contrast, Cre-expression outside of cortex is very sparse. Hypothalamic nuclei with established roles in sleep and circadian regulation show no or very few Cre-expressing cells and we found no overlap with orexin- or

melanin-concentrating hormone-expressing cells in lateral hypothalamus (Suppl. Figure 3-5). As has been shown previously, ablation of SNAP25 virtually abolishes calcium-evoked neurotransmitter release from neurons¹⁵, rendering the cells functionally silent. Importantly, normal brain development, including cortical layering and axonal path finding, has been shown in SNAP25-ablated mice¹⁵. We chose this conditional knockout mouse to probe a role for the cortex in sleep-wake regulation because in this model large and widely distributed populations of neo- and archicortical neurons involved in the generation of sleep oscillations and in the communication between cortex and subcortical structures are functionally silenced.

To investigate sleep architecture and electrophysiology in cortical SNAP25-ablated mice we performed chronic EEG, LFP, and MUA recordings as in wild type mice. Laminar MUA revealed a diminished surge of layer 5 firing at the onset of population ON periods (Figure 1g). In addition, there were significant interaction effects between genotype and cortical layer for both slow wave amplitudes ($F(1,8)=95.17$, $p<0.001$) and SWA ($F(1,8)=114.82$, $p<0.001$). The amplitude of LFP slow waves in layer 5 was decreased ($t(8)=3.70$, $p=0.006$, $d=2.34$) and the levels of slow wave activity were reduced ($t(8)=2.87$, $p=0.021$, $d=1.81$, Figure 1h,i). The opposite pattern was observed in layer 2/3, where a trend towards increased slow wave amplitudes ($t(8)=-2.21$, $p=0.058$, $d=-1.40$) and elevated slow wave activity ($t(8)=3.07$, $p=0.015$, $d=1.94$) was observed (Figure 1h,i). The differential regulation of layer 5 and 2/3 slow waves in cortical SNAP25-ablated mice results in a significantly reduced ratio of slow wave amplitudes and slow wave activity in cortical SNAP25-ablated mice (see inlays on Figure 1h,i). These layer-specific changes to intracortical dynamics are consistent with a reduction of local monosynaptic excitation between layer 5 pyramidal neurons¹⁷ and diminished disinhibitory inhibition of layer 2/3 pyramidal neurons¹⁸. Laminar firing rates and the latency to the first

spike in layer 5 were not significantly altered in cortical SNAP25-ablated mice in line with previous reports that abolition of evoked synaptic neurotransmitter release through SNAP25-ablation does not prevent neurons from depolarizing (Suppl. Figure 6)¹⁹. The profound layer-specific changes in LFP slow wave activity during NREM sleep contrasted with a lack of major differences in EEG power spectra during NREM sleep or wakefulness (Figure 1j and Suppl. Figure 7). However, cortical SNAP25-ablated mice presented a leftward shift of the EEG theta-peak frequency during REM sleep (Suppl. Figure 8). These layer- and sleep-state-specific findings underscore the importance of assessing sleep electrophysiology on the local and global levels²⁰.

Beyond the local and global changes in sleep oscillations, we observed profound genotype differences in the daily sleep-wake profile (Figure 2a). While control animals showed sleep architecture typical for wild type mice (Figure 2b)²¹, cortical SNAP25-ablated animals presented unusually long wake bouts, that often lasted several hours (Figure 2b,e). On average, conditional knockout mice spent 13.83 ± 0.39 h awake per day, approximately three hours more than controls (10.57 ± 0.42 h, $t(13)=5.55$, $p<0.001$, $d=2.96$), and the amount of sleep decreased proportionally (Figure 2c). The differences between genotypes were more pronounced in the dark period (Figure 2d and Suppl. Figure 9), which is the mouse's circadian active period but also the time of day when the homeostatic sleep drive typically builds up to high levels as a result of prolonged wakefulness²¹. This raises the question whether the increase in wakefulness is due to changes in the homeostatic or circadian process of sleep regulation.

To assess the build-up of the homeostatic sleep drive during spontaneous wakefulness, we compared the levels of EEG SWA during NREM sleep preceding and following individual wake episodes. As expected, a positive correlation was observed in both genotypes, whereby

longer spontaneous wake episodes were followed by proportionally higher levels of SWA during NREM sleep. However, the increase of SWA relative to the duration of wake episodes was smaller in conditional knockout mice compared to controls (Figure 2f, Suppl. Table 1), indicating that the relationship between sleep-wake history and the levels of SWA might be altered in cortical SNAP25-ablated animals.

An established approach to investigate the dynamics of sleep homeostasis is sleep deprivation (SD), which is most commonly performed starting at light onset, when mice in laboratory conditions usually sleep^{3,21}. Typically, SD leads to a small increase in sleep amount, especially NREM sleep, and a strong increase in sleep intensity, reflected in SWA during NREM sleep^{21,22}. However, we observed a striking difference in this homeostatic rebound between genotypes (Figure 3a-c). Although many cortical SNAP25-ablated animals had already been spontaneously awake by the time sleep deprivation started (Suppl. Figure 10a), they did not spend more time asleep after SD than controls [when sleep deprivation was performed during the first half of the light period \(Suppl. Figure 11\)](#). [When the time window of the sleep deprivation was shifted to the second half of the light period, the relative amount of sleep over the following 24 hours was reduced in cortical SNAP25-ablated mice compared to controls \(Suppl. Figure. 10b\)](#). Moreover, conditional knockout mice presented a marked attenuation of the initial increase of EEG SWA during NREM sleep after sleep deprivation (relative SWA in cortical SNAP25-ablated: 136.77 ± 3.98 %, controls: 180.57 ± 5.13 %, $t(11)=6.78$, $p<0.001$, $d=-3.87$ Figure 3b,c). Consistent with the notion of a frontal predominance of the homeostatic response to sleep deprivation²³, the genotype difference in SWA rebound was observed in the frontal EEG and LFPs, but not in the occipital EEG derivation (Suppl. Figure 12). We also observed that the increase in EEG theta-activity, a

measure of 'wake intensity', was attenuated in conditional knockout mice during SD in both the frontal and occipital EEG derivation (Suppl. Figure 13).

Since the circadian and the homeostatic process interact in the regulation of sleep and wakefulness, we next assessed whether the clock function was altered in conditional knockout mice, using a separate cohort of animals. A standard approach in circadian phenotyping consists in continuously monitoring locomotor activity using a passive infrared recording system under a 12:12 light:dark cycle followed by a release into constant darkness and exposure to a phase-advancing light pulse during the early subjective night (Circadian Time ~13.5) (Figure 3d)²⁴. We replicated the approximately three-hour difference in the amount of wakefulness in this new cohort of animals (cortical SNAP25-ablated: 11.79 ± 0.29 h, controls: 9.10 ± 0.51 h, $t(15)=4.957$, $p<0.001$, $d=2.35$) and observed that the sleep phenotype remained stable in constant darkness (Suppl. Figure 14). Importantly, cortical SNAP25-ablated animals remained rhythmic in the absence of light (Figure 3d). The free-running period was slightly shorter than 24 h and nearly identical in both genotypes (cortical SNAP25-ablated: 23.86 ± 0.04 h, controls: 23.80 ± 0.07 h, $t(15)=0.833$, $p=0.42$, $d=0.39$) and the Chi-Square periodogram analysis did not reveal any difference in circadian amplitude (Figure 3e). Finally, irrespective of genotype, the light pulse evoked a consistent phase delay, which was comparable between genotypes (Figure 3f). Taken together, our data demonstrate that cortical SNAP25 ablation leads to a diminished homeostatic sleep drive without affecting circadian regulation of sleep.

The regulation of sleep in mammals is only partially understood because it is unclear where and in what form the need to sleep is encoded, and how it is translated into an adequate compensatory response²⁵. Our study reveals a novel role for the cortex in sleep-wake regulation. We show that cortical structures actively contribute to sleep homeostasis and the

global control of vigilance states. This supports the hypothesis that brain structures fundamentally involved in sleep regulation extend far beyond the traditionally considered subcortical circuitry^{2,7,26,27}. The next step will be to understand how neo- and archicortical neurons interact with established circuits of sleep-wake control. It was recently reported that axons of layer 5 pyramidal neurons in prefrontal cortex produce an axonal terminal field in the lateral hypothalamus²⁸. Consistent with this observation, we found dense fine Cre-positive fibres surrounding cell bodies in the lateral hypothalamus (Suppl. Figure 5). Long ranging projections from prefrontal cortex, which is known to be highly sensitive to homeostatic sleep pressure²³ and a hub for the generation of slow waves during NREM sleep²⁹, might represent a direct pathway through which neocortex could modulate the vigilance states control by the lateral hypothalamus. However, layer 5 pyramidal neurons also project to thalamic nuclei, and could influence sleep regulation through corticothalamic loops^{30,31}. Given that layer 5 pyramidal neurons have a wide range of efferent connections to target structures involved in sleep-wake control, a systematic and unbiased dissection of the relevant circuits is warranted. Furthermore, a potential involvement of other neocortical cell types and of archicortical dentate gyrus cells of the hippocampus should be considered. Given the critical place of the hippocampus in brain-wide circuitry involved in memory and temporal processing, one could speculate that this structure may have a so far unrecognised role in encoding time spent awake or asleep. Targeted manipulations of the hippocampus and its neocortical projections could shed further light on the relationship between REM and NREM oscillations and their role in global sleep-wake regulation and function³².

Our results support the possibility that cortical structures generate sleep drive locally, in an activity-dependent fashion⁷, and raise the question of which mechanisms cortex could use to generate, sense and/or integrate signals of sleep need. Extracellular signals may be found in

212 molecular regulators of inflammation and plasticity⁷, or adenosine levels regulated through
213 neuro-glial interactions. Intracellular processes reflecting wake-dependent increases in sleep
214 need, conserved both in mammalian and non-mammalian species, may represent changes in
215 the synaptic phosphoproteome, endoplasmic reticulum stress, or redox homeostasis.
216 Arguably, such local signals must be integrated to elicit a global homeostatic response³³,
217 reflected in an occurrence of intense sleep, characterised by elevated cortical SWA and
218 increased sleep propensity. We propose that the wide connectivity of layer 5 pyramidal
219 neurons to other parts of cortex, thalamus, and sleep-wake regulating nuclei in
220 hypothalamus²⁸ and brainstem¹⁶, places this neuronal population in an ideal position not only
221 to generate SWA, but also to sense and integrate the signals related to sleep need, and
222 ultimately broadcast the information to the subcortical circuitry responsible for sleep-wake
223 switching¹.

Methods

Animals

Rbp4-Cre;Ai14;Snap25^{fl/fl} is a triple transgenic mouse line, which was designed as a model for functional silencing of cortical layer 5 pyramidal and dentate gyrus granule cells. Snap25^{fl/fl} is a transgene, with lox-P sites flanking the alternatively spliced exons 5a and 5b of the t-SNARE (target membrane soluble N-ethylmaleimide-sensitive factor attachment protein (SNAP) receptor) gene *Snap25*. Cre-dependent excision of exon 5a/5b leads to a reduced length gene transcript and non-detectable levels of SNAP25 protein, and cessation of Ca²⁺-dependent evoked synaptic vesicle release¹⁵. Because this chronic t-SNARE disruption allows cortex-wide silencing of selected cell types while avoiding a mechanical manipulation of cortex, which is known to affect the expression of SWA³⁴, we opted for this silencing method. In addition, our choice of this mouse model was guided by previous neurodevelopmental studies on the effects of disrupted evoked neurotransmitter release through ablation of SNARE proteins^{19,35,36} as well as by neuroanatomical work conducted in the Rbp4-Cre;Ai14;Snap25^{fl/fl} mouse line¹⁵. These studies consistently report that brain development, in particular cortical layering and axonal pathfinding, is unaffected by ablation of SNAP25^{15,19}. Moreover, as sleep homeostasis occurs on a timescale of minutes to hours, is most likely a distributed process^{33,37}, and it is not yet known whether specific areas of the cortex are more involved than others, we considered the Rbp4-Cre;Ai14;Snap25^{fl/fl} mouse model most suitable for the aims of this study¹⁶. Spontaneous behaviour appeared indistinguishable between genotypes, but conditional knockout mice have a lower body weight compared to Cre-negative controls

(cortical SNAP25-ablated: 21.3 ± 0.6 g, controls: 24.4 ± 0.6 g, $t(18)=2.94$, $p=0.009$), as reported previously¹⁵.

Chronic electrophysiological recordings

EEG/EMG implants were performed in 7 wild type C57BL/6 mice (WT, age at baseline recording 125 ± 8 days), 12 Rbp4-Cre;Ai14;Snap25^{fl/fl} mice (cKO, age at baseline recording 90 ± 5 days) and 8 Cre-negative littermates (CTR, age at baseline recording 85 ± 4 days) under isoflurane anaesthesia as described previously³⁸. For analysis of sleep architecture based on EEG/EMG recordings, 9 cKO and 6 CTR mice were included. EEG analysis of frontal and occipital spectra was conducted in 8 cKO and 5 CTR mice. Laminar LFP and MUA could be obtained across cortical layers in primary motor cortex (+ 1.1 mm AP (anterior), - 1.75 mm ML (left), tilt -15° (left)) of 7 WT, 5 cKO, and 5 CTR mice. All laminar recordings were performed using 16-channel silicon probes (NeuroNexus Technologies Inc., Ann Arbor, MI, USA; model: A1x16-3mm-100-703-Z16) with a spacing of 100 μ m between individual channels.

All mice implanted for electrophysiological recordings were housed individually in open cages before surgery and in individually ventilated cages during a recovery period of about one week after surgery. For sleep recordings, mice were transferred to separate custom-made Plexiglas cages (20.3 x 32 x 35 cm), which were placed in sound-attenuated and light-controlled Faraday chambers (Campden Instruments, Loughborough, UK), with each chamber fitting two cages. Animals were allowed free access to food pellets and water at all times and underwent daily health inspection. A 12:12 h light:dark cycle (lights on at 9 am, light levels 120–180 lux) was implemented and temperature maintained at around $22 \pm 2^\circ\text{C}$.

After an acclimatization period of at least 3 days during which animals were habituated to the tethered recording conditions, a 24 h period of continuous recording starting at light onset was performed on a designated baseline day. On the subsequent day, all animals were sleep deprived for 6 h starting at light onset. Sleep deprivation was performed during the circadian period when mice are typically asleep and thus the homeostatic response to sleep loss can be most reliably elicited²¹. At light onset, recording chambers were opened, the nesting material removed, and novel objects placed into the mouse cages to encourage exploratory behaviour. Experimenters continuously observed the mice and exchanged the provided objects for new objects when mice stopped exploring. At the end of the 6 h sleep deprivation, all objects were removed, the nesting material returned, and the recording chambers closed. Sleep deprivation was successful in both genotypes, as only a minimal amount of time (cKO: 1.84±0.75 %, CTR: 1.39±0.32 %, p=0.86 Mann-Whitney U test) was spent asleep during the 6-h interval when the mice were kept awake by providing novel objects. The electrophysiological signals revealed typical signatures of wakefulness and sleep states in both genotypes. As expected, the laminar profile of LFPs and MUAs revealed generally activated patterns during waking and rapid eye movement (REM) sleep. Correspondingly, during non-rapid eye movement (NREM) sleep, we observed depth positive LFP slow waves associated with a generalised suppression of spiking activity across cortical layers (Figure 1c)^{20,39}.

Electrophysiological acquisition, data processing, and sleep scoring

Electrophysiological in vivo recordings. Data was acquired using the 128 Channel Neurophysiology Recording System (Tucker-Davis Technologies Inc., Alachua, FL, USA) and the electrophysiological recording software Synapse (Tucker-Davis Technologies Inc.,

Alachua, FL, USA), and saved on a local computer. EEG and EMG signals were continuously recorded, filtered between 0.1 - 100 Hz, and stored at a sampling rate of 305 Hz. Extracellular neuronal activity was continuously recorded at a sampling rate of 25 kHz and filtered between 300 Hz - 5 kHz. Whenever the recorded voltage in an individual laminar channel crossed a manually set threshold indicating putative neuronal firing (at least 2 standard deviations above noise level), 46 samples around the event (0.48 ms before, 1.36 ms after) were stored. Concomitantly with the spike acquisition, LFPs were continuously recorded from the same electrodes and processed with the abovementioned settings for EEG signals.

Offline signal processing. EEG, EMG, and LFP signals were resampled at a sampling rate of 256 Hz using custom-made code in Matlab (The MathWorks Inc, Natick, Massachusetts, USA, version v2017a) and converted into the European Data Format (EDF) as previously described³⁸. Spike wave forms were further processed using a custom-made Matlab script and events with artefactual wave forms were excluded from further analysis of neuronal activity.

Scoring of vigilance states. The software Sleep Sign for Animals (SleepSign Kissei Comtec Co., Ltd., Nagano, Japan) was used for sleep scoring. EEG, EMG, and LFP recordings were partitioned into epochs of 4 s. Vigilance states were assigned manually to each recording epoch based on visual inspection of the frontal and occipital EEG derivations in conjunction with the EMG. Epochs with recording artefacts due to gross movements, chewing or external electrostatic noise were assigned to the respective vigilance state but not included in the electrophysiological analysis. Overall 18.8 ± 3.5 % of wake, 0.7 ± 0.4 % of NREM, and 0.9 ± 0.4 % of REM epochs contained artefactual EEG signals across all animals included in the EEG spectral analysis, with no significant difference between genotypes. EEG and LFP power

spectra were computed using a fast Fourier transform routine (Hanning window) with a 0.25 Hz resolution and exported in the frequency range between 0 and 30 Hz for spectral analysis.

Non-invasive measurement of home cage activity for circadian phenotyping

Circadian characteristics were assessed in a separate cohort of 10 cKO (age at baseline recording 84 ± 1 days) and 7 CTR mice (age at baseline recording 83 ± 1 days). These mice were housed individually and placed under a passive infrared motion detector that continuously recorded activity in time intervals of 100 ms. Individual readings were pooled into one minute bins for all analyses as it has previously been validated that periods of inactivity of >40 s provide a reliable measure of behaviourally defined sleep⁴⁰. Mice were housed in a stable 12:12 h light:dark cycle for at least 7 days before being released into constant darkness. The circadian period and amplitude were assessed over an interval of 7-10 days in the constant dark condition by ChiSquare periodogram analysis using ActogramJ⁴¹. After at least 10 days in constant darkness, all mice were exposed to a 2h light pulse provided around Circadian Time 13.5 h. The resulting phase delay of the circadian rhythm was quantified in all animals by extrapolating the onsets of activity to the day of the light pulse²⁴.

Statistical analyses

Data were analysed using MATLAB (version R2017b; The MathWorks Inc, Natick, MA, USA), SAS JMP (version 7.0; SAS Institute Inc. Cary, NC, USA) and IBM SPSS Statistics for Windows (version 25.0; IBM Corp., Armonk, N.Y., USA). Reported averages are mean \pm s.e.m. Analyses of variance (ANOVAs) were performed as described in Howell and Lacroix (2012)⁴². To examine potential differences in firing dynamics between superficial versus deep cortical layers in WT animals, repeated-measures ANOVAs were conducted with cortical layers (layer

2/3 versus layer 5) and time bins as within-subject factors. To examine potential differences between genotypes, split-plot ANOVAs were conducted; genotype (CTR versus cKO animals) was entered as a between-subject factor, whereas time bins, EEG spectral bins, and vigilance states (wake, NREM, and REM) were entered as within-subject factors. $\alpha = 0.05$ was adopted for main effects and interactions. Significant two-way interaction terms were followed up with Bonferroni-adjusted post hoc comparisons with $\alpha_{\text{adjusted}} = 0.05/k$, where k represents the total number of pairwise comparisons made⁴³. In ANOVAs with multiple time points, the total number of post hoc comparisons was minimised in each case, and hence controlling for the increase in familywise error rate, by pooling across multiple time bins (e.g., 0–10 ms, 11–20 ms, and 21–30 ms in Figure 1g). For spectral analysis, EEG/LFP power spectra of individual animals were log-transformed before hypothesis testing. Bonferroni correction was not applied for post hoc comparison of spectral data because ANOVAs consisting of 119 EEG spectral bins would be too conservative and reduce statistical power⁴⁴; thus, α was kept at 0.05 in these cases. In the summary of statistical methods and results (Suppl. Table 1) we report frequency bins with significant differences in post-hoc comparison before ($\alpha_{\text{uncorrected}}$) and after Bonferroni adjustment of α ($\alpha_{\text{corrected}}$). In all figure panels illustrating EEG or LFP spectrograms, frequency bins for which the resulting post-hoc comparison was significant after Bonferroni adjustment are highlighted with black asterisks; bins only significant before Bonferroni adjustment are highlighted with grey asterisks to indicate areas of interest bearing in mind that no correction for multiple comparisons was applied. In the circadian analysis, a multivariate ANOVA (MANOVA) was conducted to examine if the linear combination of multiple circadian response variables (period length, periodogram power, and phase shift) differed between genotypes⁴⁵. Greenhouse-Geisser correction was used when the assumption of sphericity was violated (Mauchly's test of sphericity, $p < 0.05$). Mann-Whitney

U tests were performed for main analyses instead of one-way ANOVAs if the assumption of normality was violated (Shapiro-Wilk test of normality, $p < 0.05$). The statistical methods and results from each individual analysis are listed in supplementary table 1. In all figures, significance levels are indicated with black asterisks: '*' for $0.05 \geq p > 0.01$; '**' for $0.01 \geq p > 0.001$; '***' for $0.001 \geq p$. Grey asterisks indicate post-hoc comparisons with $P < 0.05$, which do not reach significance after Bonferroni-correction for multiple comparisons. Panels representing grouped data of durations spent in specific vigilance states show group mean (red line), 95% confidence interval (pink box), and one standard deviation (blue box) with individual data points overlaid; these plots were generated using the MATLAB function `notBoxPlot` (Rob Campbell (2019). `notBoxPlot` (<https://www.github.com/raacampbell/notBoxPlot>), GitHub. Retrieved June 15, 2019). For key analyses reported in the main text, the effect sizes are reported as Cohen's d calculated using the MATLAB function `computeCohen_d` (Ruggero G. Bettinardi (2021). `computeCohen_d(x1, x2, varargin)` (https://www.mathworks.com/matlabcentral/fileexchange/62957-computecohen_d-x1-x2-varargin), MATLAB Central File Exchange. Retrieved October 4, 2020).

Electrophysiological criteria for analysis of vigilance state episodes and OFF periods

For analyses of mean and maximum duration of sustained wake episodes in the EEG dataset (Figure 2e), we included wake episodes, which were at least 1 min long allowing brief intrusions of sleep of 1 min or less. For the analysis of mean duration of NREM episodes, we included NREM episodes, which were at least 1 min long allowing brief intrusions of REM sleep or brief awakenings of 1 min or less (Suppl. Figure11). To investigate the change in NREM SWA across prolonged wake episodes under undisturbed conditions, we used the EEG

dataset from the baseline day and included consolidated periods of waking lasting at least 15 min, whereby short episodes of sleep <1 min were not considered as interruptions. We then performed analyses of NREM sleep SWA in the 15-min time window immediately preceding and following prolonged (>15 min) wake episodes, if both time windows included at least 10 min of artefact-free NREM sleep and no more than 3 min of wakefulness (Figure 2f). Population OFF periods were defined as periods of total neuronal silence across all electrodes, which lasted at least 50 ms and no more than 4000 ms. Subsequently, the top 20% longest OFF periods were included for final analyses (Figure 1g,h and Suppl. Figure 1). The latency to the first spike after the population OFF-ON transition was calculated separately for MUA recorded in layers 2/3 and layer 5. Only ON periods with at least 1 spike in each of the layers occurring within the first 200 ms were included in this analysis (Suppl. Figure 1).

Histological assessment of laminar probe depth

The tips of laminar implants were stained before surgery with the orange-red fluorescent membrane stain Dil[®] (1,1'-Diocadecyl-3,3,3',3'-Tetramethylindocarbocyanine Perchlorate; Thermo Fisher Scientific, Waltham, MA, USA) by immersion of the electrode shank into a 20 mg/ml solution (50/50% acetone/methanol) for later histological assessment of the electrode position⁴⁶. After completion of the experiments, microlesions of selected channels on the laminar probe were performed under terminal pentobarbital anaesthesia using the electroplating device NanoZTM (White Matter LLC, Seattle, WA, USA) applying 10 mA direct current for 25 s to each respective channel. Immediately following microlesioning, mice were perfused with 0.1M phosphate buffered saline (0.9 %) (PBS) followed by 4 % paraformaldehyde in PBS for tissue preservation. A vibrating microtome (Leica VT1000S) was

used to section the brains into 50 μ m coronal slices. Fluorescent staining was performed with 4',6-diamidino-2-phenylindole (DAPI). After fluorescence microscopy, implantation sites were mapped using a mouse brain atlas⁴⁷ and the depth of the laminar implant was assessed measuring the distance between cortical surface and the electrical current induced tissue microlesions. ImageJ was used to merge fluorescence images and add scale bars⁴⁸.

Histological assessment of Cre-expression in cortex, dentate gyrus, and hypothalamus

Coronal brain sections from six Rbp4-Cre;Ai14;Snap25^{fl/+} mice were prepared using the same procedure as outlined above for the histological assessment of the laminar probe depth. Laser scanning confocal microscope images were acquired (Zeiss LSM710) and image stacks created to assess the cellular morphology across the z-plane of the brain section. The cytoplasmic tdTomato expressed from the *Ai14* reporter gene allows reliable identification of Cre+ neurons based on native tdTomato fluorescence^{15,49}. The native fluorescence is detectable even in thin neurites and synapses, which can be used to visualise the dendritic and axonal morphology of labelled neurons.

Immunohistochemistry to determine lateral hypothalamic cell identity

To determine whether Cre+ neurons in the lateral hypothalamus express melanin concentrating hormone (MCH) or orexin/hypocretin (Hcrt), coronal sections from three Rbp4-Cre;Ai14 were prepared as described above. Before counterstaining with DAPI, the sections were stained with rabbit anti-MCH antibody (1:2000; H-070-47; Phoenix Pharmaceuticals) or rabbit anti-Hcrt antibody (1:500, kind gift from Anthony Van den Pol, Yale University). Briefly, sections were incubated in blocking solution (3% or 10% donkey serum [Hcrt or MCH respectively] and 0.3% Triton-X100 in 0.1M PBS) for one hour before incubation with the

primary antibody in blocking solution at 4°C overnight (MCH) or for 72h (Hcrt). The primary antibody was revealed by incubating with donkey anti-rabbit-AlexaFluor488 (1:500) antibody in blocking solution for two hours at room temperature. Subsequently, epifluorescence and confocal imaging was performed as described above.

Ethical approval

All experiments were performed in accordance with the United Kingdom Animal Scientific Procedures Act 1986 under personal and project licences granted by the United Kingdom Home Office. Ethical approval was provided by the Ethical Review Panel at the University of Oxford. Animal holding and experimentation were located at the Biomedical Sciences Building (BSB) and the Behavioural Neuroscience Unit (BNU), University of Oxford.

Code availability

Custom-made code for data analysis used in this study is available from the corresponding authors upon request.

Data availability

The datasets acquired for this study are available from the corresponding authors upon request.

References

- 457 1. Saper, C. B. & Fuller, P. M. Wake–sleep circuitry: an overview. *Curr. Opin. Neurobiol.*
458 **44**, 186–192 (2017).
- 459 2. Liu, D. & Dan, Y. A Motor Theory of Sleep-Wake Control: Arousal-Action Circuit. *Annu.*
460 *Rev. Neurosci.* **42**, 27–46 (2019).
- 461 3. Vyazovskiy, V. V. *et al.* Cortical Firing and Sleep Homeostasis. *Neuron* **63**, 865–878
462 (2009).
- 463 4. Borbély, A. A., Daan, S., Wirz-Justice, A. & Deboer, T. The two-process model of sleep
464 regulation: A reappraisal. *J. Sleep Res.* **25**, 131–143 (2016).
- 465 5. Huber, R., Felice Ghilardi, M., Massimini, M. & Tononi, G. Local sleep and learning.
466 *Nature* **430**, 78–81 (2004).
- 467 6. Vyazovskiy, V. V. *et al.* Local sleep in awake rats. *Nature* **472**, 443–7 (2011).
- 468 7. Krueger, J., Nguyen, J. T., Dykstra-Aiello, C. J. & Taishi, P. Local sleep. *Sleep Med. Rev.*
469 **43**, 14–21 (2019).
- 470 8. Krone, L. B. & Vyazovskiy, V. V. Unresponsive or just asleep? Do local slow waves in
471 the perilesional cortex have a function? *Brain* **143**, 3513–3515 (2020).
- 472 9. Beltramo, R. *et al.* Layer-specific excitatory circuits differentially control recurrent
473 network dynamics in the neocortex. *Nat. Neurosci.* **16**, 227–234 (2013).
- 474 10. Chauvette, S., Volgushev, M. & Timofeev, I. Origin of Active States in Local Neocortical
475 Networks during Slow Sleep Oscillation. *Cereb. Cortex* **20**, 2660–2674 (2010).
- 476 11. Sanchez-Vives, M. V & McCormick, D. A. Cellular and network mechanisms of rhythmic
477 recurrent activity in neocortex. *Nat. Neurosci.* **3**, 1027–1034 (2000).
- 478 12. Buzsáki, G. Theta Oscillations in the Hippocampus. *Neuron* **33**, 325–340 (2002).
- 479 13. Boyce, R., Glasgow, S. D., Williams, S. & Adamantidis, A. Causal evidence for the role
480 of REM sleep theta rhythm in contextual memory consolidation. *Science* **352**, 812 LP –

481 816 (2016).

482 14. Sanchez-Vives, McCormick, D. A., Sanchez-Vives, M. V & McCormick, D. A. Cellular
483 and network mechanisms of rhythmic recurrent activity in neocortex. *Nat. Neurosci.*
484 **3**, 1027–1034 (2000).

485 15. Hoerder-Suabedissen, A. *et al.* Cell-Specific Loss of SNAP25 from Cortical Projection
486 Neurons Allows Normal Development but Causes Subsequent Neurodegeneration.
487 *Cereb. Cortex* **29**, 2148–2159 (2019).

488 16. Gerfen, C. R., Paletzki, R. & Heintz, N. GENSAT BAC cre-recombinase driver lines to
489 study the functional organization of cerebral cortical and basal ganglia circuits.
490 *Neuron* **80**, 1368–1383 (2013).

491 17. Lefort, S., Tómm, C., Floyd Sarria, J.-C. & Petersen, C. C. H. The Excitatory Neuronal
492 Network of the C2 Barrel Column in Mouse Primary Somatosensory Cortex. *Neuron*
493 **61**, 301–316 (2009).

494 18. Vecchia, D. *et al.* Temporal Sharpening of Sensory Responses by Layer V in the Mouse
495 Primary Somatosensory Cortex. *Curr. Biol.* **30**, 1589-1599.e10 (2020).

496 19. Washbourne, P. *et al.* Genetic ablation of the t-SNARE SNAP-25 distinguishes
497 mechanisms of neuroexocytosis. *Nat. Neurosci.* **5**, 19–26 (2002).

498 20. Funk, C. M., Honjoh, S., Rodriguez, A. V., Cirelli, C. & Tononi, G. Local slow waves in
499 superficial layers of primary cortical areas during REM sleep. *Curr. Biol.* **26**, 396–403
500 (2016).

501 21. Huber, R., Deboer, T. & Tobler, I. Effects of sleep deprivation on sleep and sleep EEG
502 in three mouse strains: empirical data and simulations. *Brain Res.* **857**, 8–19 (2000).

503 22. Franken, P., Dijk, D. J., Tobler, I. & Borbely, A. A. Sleep deprivation in rats: effects on
504 EEG power spectra, vigilance states, and cortical temperature. *Am. J. Physiol. Integr.*

505 *Comp. Physiol.* **261**, R198–R208 (1991).

506 23. Huber, R., Deboer, T. & Tobler, I. Topography of EEG Dynamics After Sleep
507 Deprivation in Mice. *J. Neurophysiol.* **84**, 1888–1893 (2000).

508 24. Albrecht, U. & Foster, R. G. Placing ocular mutants into a functional context: a
509 chronobiological approach. *Methods* **28**, 465–477 (2002).

510 25. Frank, M. G. & Heller, H. C. The Function(s) of Sleep. *Handbook of Experimental*
511 *Pharmacology* **253**, 3–34 (2019).

512 26. Morairty, S. R. *et al.* A role for cortical nNOS/NK1 neurons in coupling homeostatic
513 sleep drive to EEG slow wave activity. *Proc Natl Acad Sci U S A* **110**, 20272–20277
514 (2013).

515 27. Tossell, K. *et al.* Sleep deprivation triggers somatostatin neurons in prefrontal cortex
516 to initiate nesting and sleep via the preoptic and lateral hypothalamus. *bioRxiv*
517 2020.07.01.179671 (2020). doi:10.1101/2020.07.01.179671

518 28. Prasad, J. A., Carroll, B. J. & Sherman, S. M. Layer 5 Corticofugal Projections from
519 Diverse Cortical Areas: Variations on a Pattern of Thalamic and Extrathalamic Targets.
520 *J. Neurosci.* **40**, 5785 LP – 5796 (2020).

521 29. Massimini, M., Huber, R., Ferrarelli, F., Hill, S. & Tononi, G. The sleep slow oscillation
522 as a traveling wave. *J. Neurosci.* **24**, 6862–70 (2004).

523 30. Krone, L. *et al.* Top-down control of arousal and sleep: Fundamentals and clinical
524 implications. *Sleep Med. Rev.* **31**, 17–24 (2017).

525 31. Gent, T. C., Bandarabadi, M., Herrera, C. G. & Adamantidis, A. Thalamic dual control
526 of sleep and wakefulness. *Nat. Neurosci.* **21**, 974–984 (2018).

527 32. Hayashi, Y. *et al.* Cells of a common developmental origin regulate REM/non-REM
528 sleep and wakefulness in mice. *Science* **350**, 957 LP – 961 (2015).

- 529 33. Thomas, C. W., Guillaumin, M. C. C., McKillop, L. E., Achermann, P. & Vyazovskiy, V. V.
530 Global sleep homeostasis reflects temporally and spatially integrated local cortical
531 neuronal activity. *Elife* **9**, e54148 (2020).
- 532 34. Sheroziya, M. & Timofeev, I. Global intracellular slow-wave dynamics of the
533 thalamocortical system. *J. Neurosci.* **34**, 8875–8893 (2014).
- 534 35. Verhage, M. *et al.* Synaptic Assembly of the Brain in the Absence of Neurotransmitter
535 Secretion. *Science* **287**, 864 LP – 869 (2000).
- 536 36. Molnár, Z. *et al.* Normal Development of Embryonic Thalamocortical Connectivity in
537 the Absence of Evoked Synaptic Activity. *J. Neurosci.* **22**, 10313 LP – 10323 (2002).
- 538 37. Krueger, J. & Obál, F. A neuronal group theory of sleep function. *J. Sleep Res.* **2**, 63–69
539 (1993).
- 540 38. McKillop, L. E. *et al.* Effects of Aging on Cortical Neural Dynamics and Local Sleep
541 Homeostasis in Mice. *J. Neurosci.* **38**, 3911 LP – 3928 (2018).
- 542 39. Sakata, S. & Harris, K. D. Laminar Structure of Spontaneous and Sensory-Evoked
543 Population Activity in Auditory Cortex. *Neuron* **64**, 404–418 (2009).
- 544 40. Brown, L., Hasan, S., Foster, R. G. & Peirson, S. N. COMPASS: Continuous Open Mouse
545 Phenotyping of Activity and Sleep Status. *Wellcome open Res.* **1**, 2 (2016).
- 546 41. Schmid, B., Helfrich-Förster, C. & Yoshii, T. A New ImageJ Plug-in “ActogramJ” for
547 Chronobiological Analyses. *J. Biol. Rhythms* **26**, 464–467 (2011).
- 548 42. Howell, G. T. & Lacroix, G. L. Decomposing interactions using GLM in combination
549 with the COMPARE, LMATRIX and MMATRIX subcommands in SPSS. *Tutor. Quant.*
550 *Methods Psychol.* **8**, 1–22 (2012).
- 551 43. Howell, D. C. *Statistical Methods for Psychology*. (Cengage Learning, 2012).
- 552 44. Achermann, P. & Borbély, A. A. Coherence analysis of the human sleep

553 electroencephalogram. *Neuroscience* **85**, 1195–1208 (1998).

554 45. Tabachnick, B. & Fidell, L. Multivariate Analysis of Variance (MANOVA). in

555 *International Encyclopedia of Statistical Science* (2011).

556 46. Magill, P. J. *et al.* Changes in Functional Connectivity within the Rat Striatopallidal Axis

557 during Global Brain Activation In Vivo. *J. Neurosci.* **26**, 6318–6329 (2006).

558 47. Paxinos, G. & Franklin, K. B. J. *Paxinos and Franklin's the mouse brain in stereotaxic*

559 *coordinates*. (Elsevier Academic Press, 2019).

560 48. Schindelin, J. *et al.* Fiji: an open source platform for biological image analysis. *Nat.*

561 *Methods* **9**, 676–682 (2012).

562 49. Grant, E., Hoerder-Suabedissen, A. & Molnar, Z. The Regulation of Corticofugal Fiber

563 Targeting by Retinal Inputs. *Cereb. Cortex* **26**, 1336–1348 (2016).

564

565

Acknowledgements

We thank Thomas Jahans-Price and Xudong Wang for their help with establishing the microlesion protocol; Merima Sabanovic for her advice on statistics and figure production; Kristina Parley for her support in the histological procedures; all members of the Vyazovskiy lab for their kind help with surgery assistance, animal care, and sleep deprivation. We are very grateful to Ed Mann, University of Oxford, for his advice on the laminar analysis and to Anthony Van den Pol, Yale University, for his generous gift of rabbit anti-Hcrt antibody. This work was supported by the Wellcome Trust PhD studentships 203971/Z/16/Z to LBK and 109059/Z/15/Z to CBD. MCK was supported by a Berrow Foundation Lord Florey Scholarship. VvdV and LMCK were supported by Novo Nordisk Postdoctoral Fellowships run in partnership with the University of Oxford. This work was further supported by a Wellcome Trust Strategic Award 098461/Z/12/Z, John Fell OUP Research Fund Grant 131/032, and Medical Research Council (UK) grant MR/N026039/1.

Author contributions

ZM and VVV initiated and proposed the study with pilot experiments done by TY. LBK, TY, CJA, AHS, ZM, and VVV designed the experiments. LBK, TY, MCCG, and CBD conducted the electrophysiological experiments on the transgenic mouse model. LBK, CBD, and MCK conducted the electrophysiological experiments on wild type mice. LBK, VvdV, LMCK, SKET, and SNP conducted and analysed the passive infrared recordings on the transgenic mouse model. LBK, MCK, and AHS performed the histology. AHS and ZM developed, validated, and provided the transgenic mice. LBK, VvdV, SKET, and VVV analysed the data. LBK and VVV

588 wrote the manuscript. All of the authors discussed the results and commented on the
589 manuscript.

590

591 **Competing interests**

592 The authors declare no competing interests.

593

594 **Figures**

595

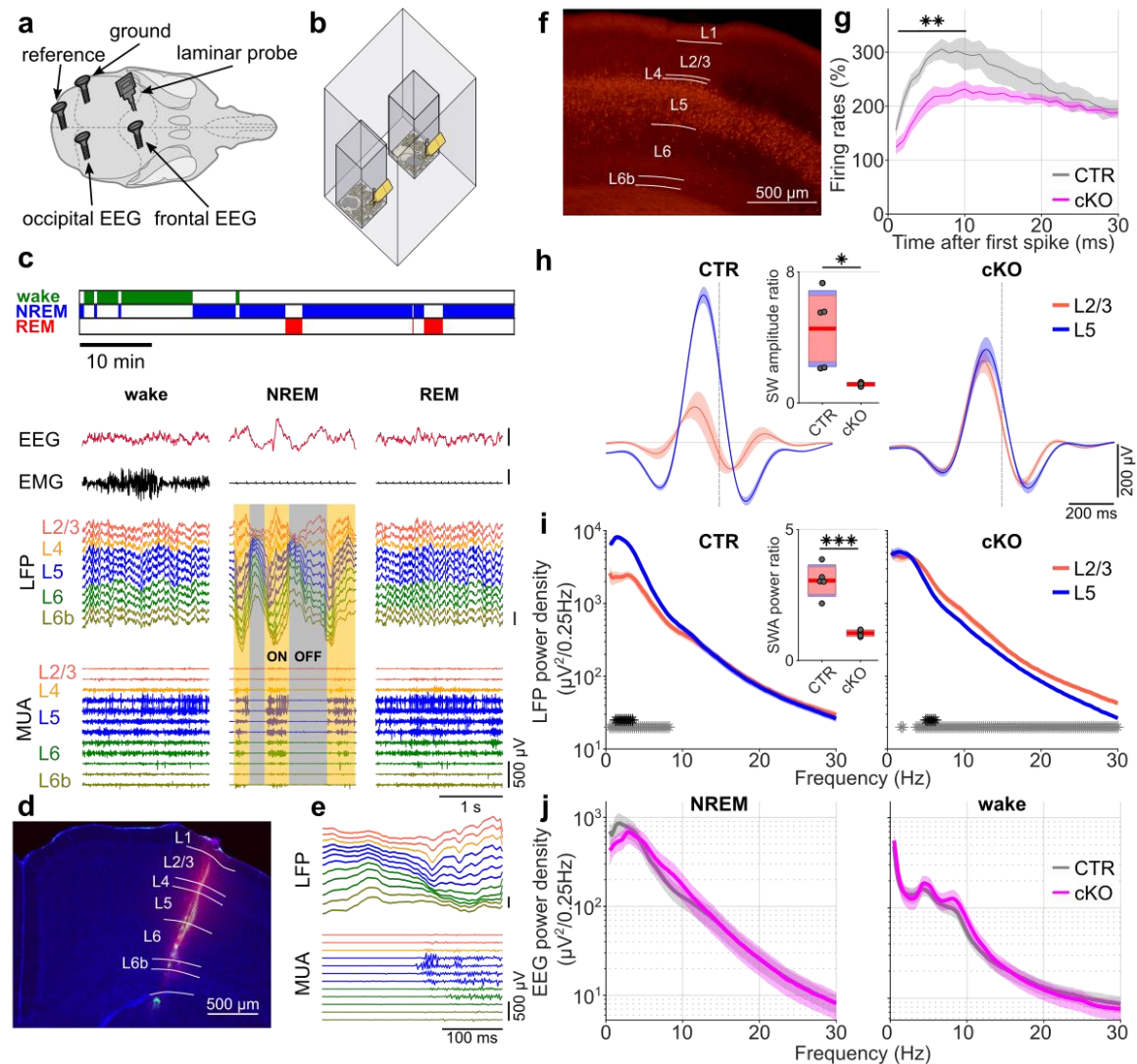


Figure 1: Cortical recordings in freely moving mice implicate layer 5 in the generation of slow waves during NREM sleep.

a) Schematic of the mouse skull showing EEG/LFP electrode positions. b) Schematic of the recording chamber with two Plexiglas cages for recording of individually housed mice. c) Representative hypnogram colour coded for the three vigilance states (wake, NREM, and REM sleep) and corresponding EEG, EMG, LFP, and MUA traces. Neuronal ON and OFF periods during NREM sleep are highlighted with transparent yellow and grey panels, respectively. All scale bars on y-axis, 500μV. d) Representative histology image showing a DAPI counterstained (blue) coronal section of the mouse brain. The Dil trace (red) indicates the electrode insertion tract reaching just below the corpus callosum. Merged image using three fluorescent channels. e) Representative OFF-ON transition illustrating that population activity typically starts in layer 5. Channel assignment and colour coding correspond to panel (c). Both scale bars on y-axis, 500μV. f) Representative histology of neocortical Cre-expression under the Rbp4-Cre promoter. Note that Cre-positive cells (red) in neocortex are largely restricted to layer 5. g) Neuronal activity in layer 5 (L5) at OFF-ON transitions in cortical Snap25-ablated (cKO) and Cre-negative control (CTR) animals relative to NREM sleep average. h) Average LFP slow wave in layers 2/3 (L2/3) and 5 aligned to the OFF-ON transition (vertical dashed line) in cKO and CTR mice. *The inset illustrates the significant*

genotype difference in slow wave (SW) amplitude ratio between L2/3 and L5. i) LFP spectra of L2/3 and L5 of cKO and CTR mice during NREM sleep. Individual asterisks indicate frequency bins with significant differences in post-hoc comparison before (grey) and after (black) Bonferroni adjustment of α . The inlay illustrates the significant genotype difference in slow wave activity (SWA) ratio between L2/3 and L5. j) Frontal EEG spectra of both genotypes during NREM sleep and wakefulness.

Number of animals: n=5 CTR and n=5 cKO for laminar analysis (panels g-i), n=5 CTR and n=8 cKO for EEG spectral analysis (panel j). Black asterisks indicate post-hoc contrasts with significant differences (* $p < 0.05$, ** $p < 0.01$, *** $p < 0.001$). Statistical methods and results for all analyses provided in Suppl. Table 1.

cKO: conditional knockout animals. CTR: control animals. Dil: 1,1'-Diocetadecyl-3,3,3',3'-Tetramethylindocarbocyanine Perchlorate. EEG: electroencephalogram. EMG: electromyogram. L2/3, L5: Neocortical layers 2/3, 5. LFP: local field potentials. MUA: multi unit activity. NREM: non-rapid eye movement sleep. REM: rapid eye movement sleep. WT: wild type animals.

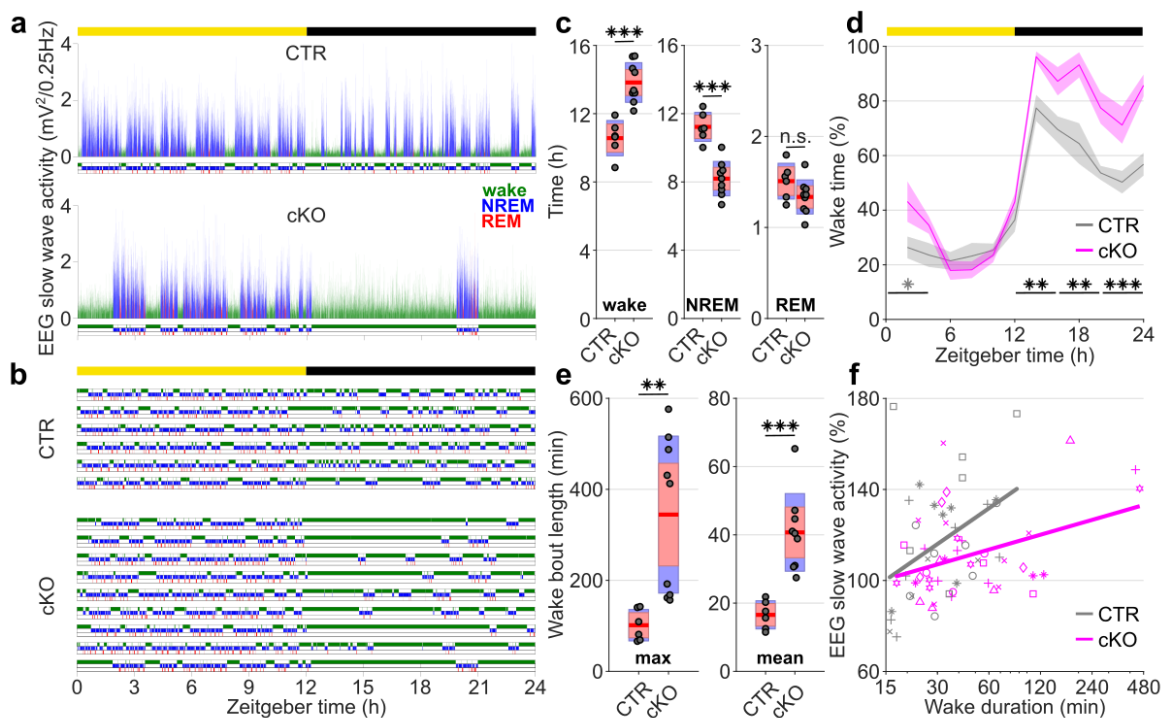


Figure 2: Selective cortical SNAP25 ablation alters sleep architecture.

a) Hypnogram and EEG slow wave activity (0.5- 4.0Hz, 4s epochs) of one representative animal from each genotype in undisturbed 24h baseline recordings. b) Hypnograms from all individual Cre-negative control (CTR) and cortical SNAP25-ablated (cKO) animals under undisturbed baseline conditions. Note the increased amount of wakefulness and long wake episodes in cKOs. Vigilance states in a&b colour coded: wake=green, NREM=blue, REM=red. c) Time spent in vigilance states (wake, NREM, and REM) during 24h baseline recordings. d) Time course of wakefulness over 24h baseline recordings, showing that the differences between genotypes mostly occur during the dark period (ZT12-24). e) Maximum and mean duration of all spontaneous wake episodes over the 2-day recording period, excluding the 6 h sleep deprivation. f) Relationship between wake duration and relative SWA in the frontal

EEG derivation during NREM epochs on baseline day. Individual animals are represented with different symbols.

Number of animals: n=6 CTR and n=9 cKO for vigilance state analysis (panels c, d, e), n=5 CTR and n=8 cKO for EEG spectral analysis (panel f). Black asterisks indicate post-hoc contrasts with significant differences ($*P < 0.05$, $**P < 0.01$, $***P < 0.001$), grey asterisk indicates post-hoc comparison with $P < 0.05$, which does not reach significance after Bonferroni correction for multiple comparisons. Statistical methods and results for all analyses provided in Suppl. Table 1. Yellow and black bars above panels a, b and d indicate light and dark periods, respectively. Panels c and e represent grouped data including group mean (red line), 95% confidence interval (pink box), and one standard deviation (blue box) with individual data points overlaid.

BL: baseline. cKO: conditional knockout animals. CTR: control animals. EEG: electroencephalogram. NREM: non-rapid eye movement sleep. REM: rapid eye movement sleep. SD: sleep deprivation. ZT: zeitgeber time.

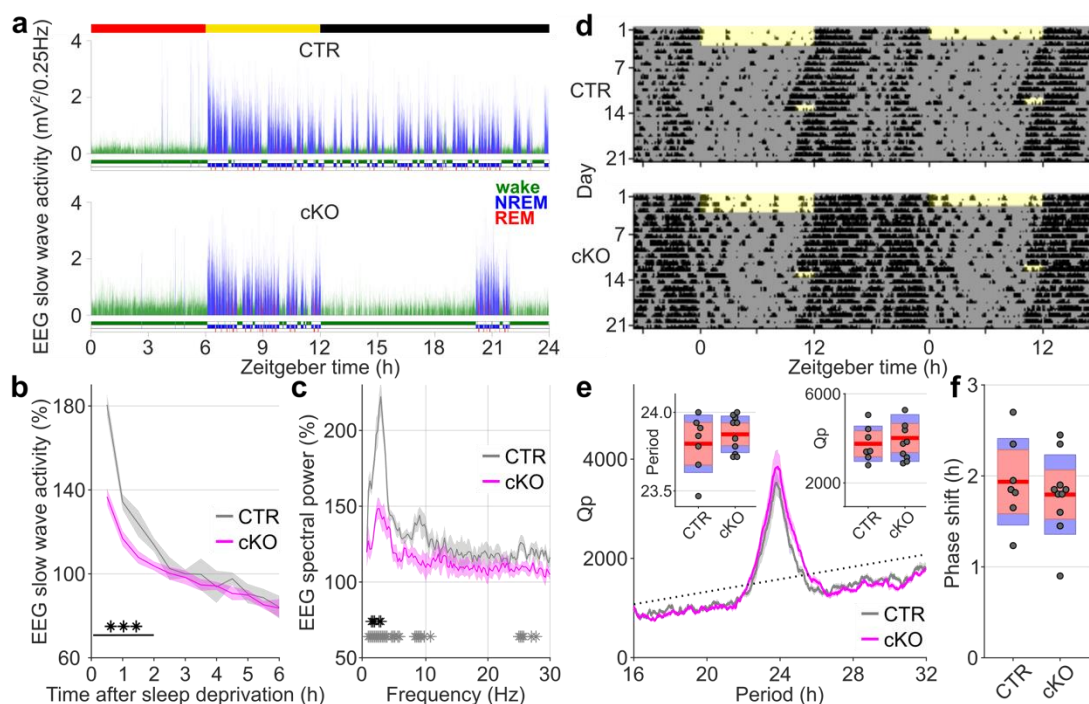
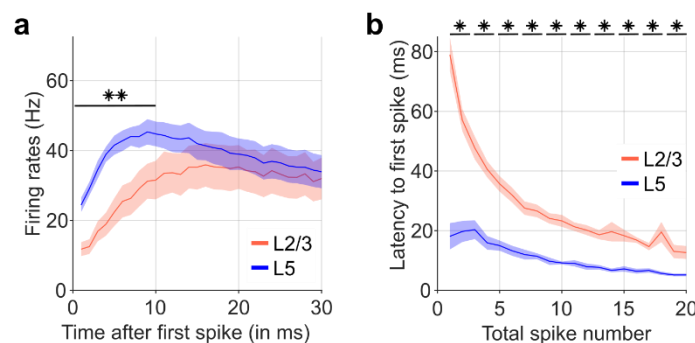


Figure 3: Selective cortical SNAP25 ablation alters homeostatic but not circadian sleep regulation.

a-c) Homeostatic response to 6h sleep deprivation at light onset based on EEG spectral analysis. a) Hypnogram and EEG slow wave activity (0.5- 4.0Hz, 4s epochs) of one representative animal from each genotype in 24h recordings with 6h sleep deprivation (red, yellow and black bars indicate sleep deprivation, light and dark periods, respectively). b) Time course of frontal EEG slow wave activity during NREM sleep after sleep deprivation relative to baseline average. Note that during the first 2 hours after sleep deprivation cortical Snap25-ablated (cKO) animals show lower levels of SWA compared to Cre-negative controls (CTR). c) Spectral power in the frontal EEG of NREM sleep during the first 30 minutes after sleep deprivation relative to baseline NREM average. Individual asterisks indicate frequency bins with significant differences in post-hoc comparison before (grey) and after (black) Bonferroni adjustment of α . **d-f) Circadian phenotyping based on passive**

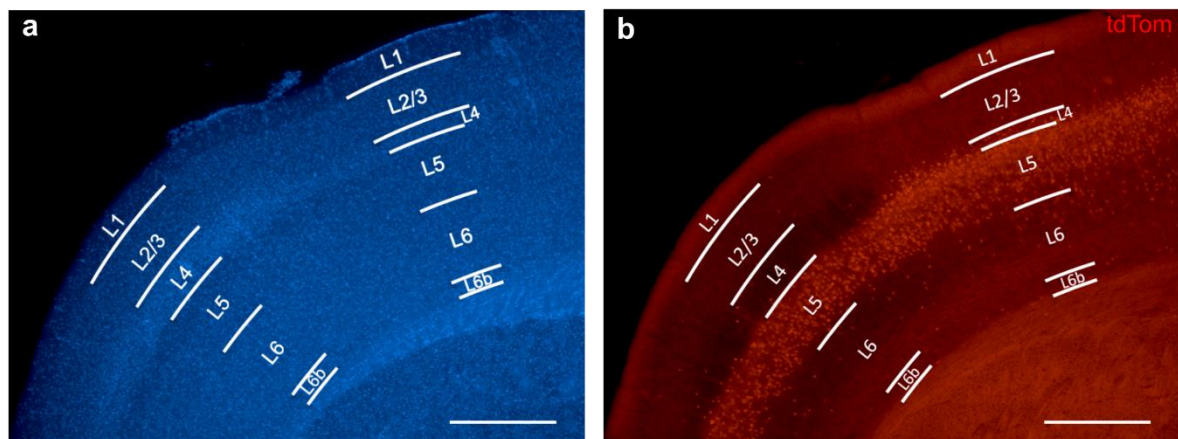
infrared recordings (PIR). d) Representative actograms of one CTR and one cKO mouse. Day 1-3: 12:12h LD cycle. From day 4: constant darkness protocol. Day 13: a phase-delaying 2h light pulse is provided. e) Average Chi-square periodogram. Insets: period (h) and periodogram power (Qp). f) Phase shift in activity onset on the day after the light pulse. No significant differences were observed in any of the assessed circadian characteristics. Number of animals: n=5 CTR and n=8 cKO for EEG spectral analysis (panel b,c), n=7 CTR and n=10 cKO for PIR analysis (panels e,f). Black asterisks indicate post-hoc contrasts with significant differences ($*p < 0.05$, $**p < 0.01$, $***p < 0.001$). Statistical methods and results for all analyses provided in Suppl. Table 1. Panels e and f represent grouped data including group mean (red line), 95% confidence interval (pink box), and one standard deviation (blue box) with individual data points overlaid. cKO: conditional knockout animals. CTR: control animals. EEG: electroencephalogram. LD: light:dark. NREM: Non-rapid eye movement sleep. PIR: passive infrared recordings. SWA: Slow wave activity (0.5- 4.0Hz).



Suppl. Figure 1: Neuronal dynamics around OFF-ON transitions imply a leading role of layer 5 in population activity.

a) Average neuronal firing activity at the transitions from population OFF to ON periods during baseline NREM sleep. Note that firing rates at the OFF-ON transition are higher in layer 5 during the first 10ms after the first spike. b) Latency to the first spike for matched spike numbers during the first 200ms of the ON period. Note that the latency to the first spike is shorter in layer 5 irrespective of the total number of spikes in a given ON period. N=7 wild type (C57L/6) mice. Black asterisks indicate post-hoc contrasts with significant differences ($*p < 0.05$, $**p < 0.01$, $***p < 0.001$). Statistical methods and results provided in Suppl. Table 1. Number of animals: L2/3, L5: Neocortical layers 2/3, 5. NREM: non-rapid eye movement sleep.

700



701

702

703

704

705

706

707

708

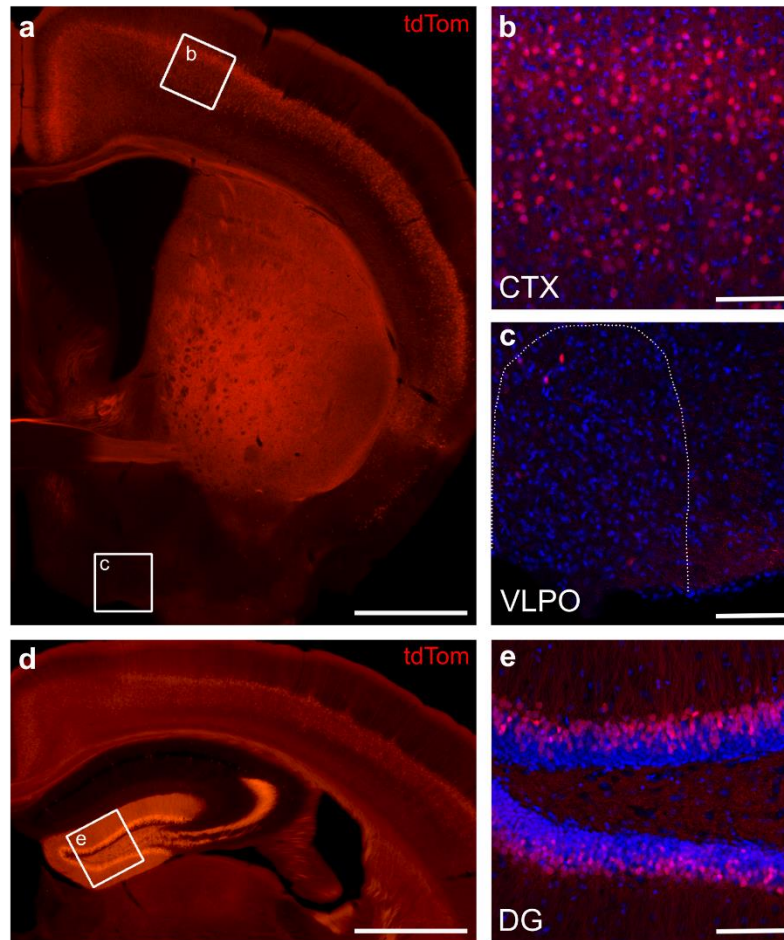
709

710

Suppl. Figure 2: Identification of cortical layers in a representative coronal brain slice covering primary motor and sensory cortex.

a) Cortical layers were determined using DAPI staining and identification of characteristic anatomical features of specific layers such as cell density and nuclear size. b) Image shows that expression of the red fluorescent protein tdTomato is restricted to layer 5 in both primary motor and sensory cortex. The selective Cre-expression was driven by a Rbp4 promoter that cleaved the STOP-floxed site in the tdTomato reporter Ai14 mouse. Anterior-posterior position: approximately Bregma +0.75 mm.

DAPI: 4',6-diamidino-2-phenylindole. Scale bars: 500 μ m.

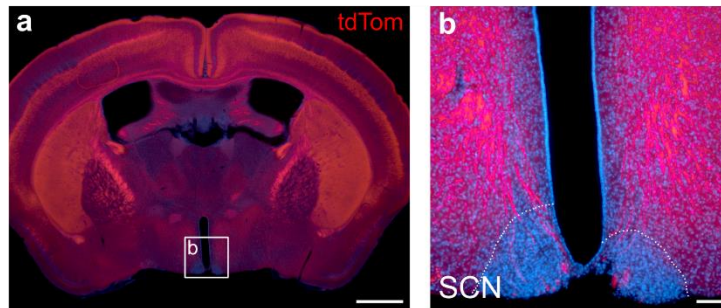


Suppl. Figure 3: Comparison of Cre-expression in the Rbp4-Cre mouse line between neocortical layer 5, dentate gyrus and hypothalamus.

a) Coronal section of an Rbp4-Cre;Ai14;Snap25^{fl/+} mouse brain indicating areas, which were further examined for Cre-expression using confocal imaging of DAPI stained slices. b,c) Laser scanning confocal microscope images from neocortex (CTX, b) and ventrolateral preoptic hypothalamus (VLPO, c) of DAPI stained (blue) sections, showing the distribution of tdTomato+ cells in the two regions. The VLPO region is outlined with a white, dotted line. Cell counts on corresponding coronal sections in three brains revealed that $20.53 \pm 0.98\%$ (480/2342) of cortical L5 cells were tdTomato+, while only $1.15 \pm 0.40\%$ (35/3006) of hypothalamic cells expressed the red fluorescent indicator. d) Coronal section of an Rbp4-Cre;Ai14;Snap25^{fl/+} mouse brain indicating the area of the dentate gyrus which was further examined for Cre-expression. e) Laser scanning confocal microscope image of dentate gyrus (DG) in a DAPI stained (blue) section. TdTomato+ cells were quantified in both the top and bottom blades of DG in three images, each from three different brains, and comprise $39.39 \pm 3.72\%$ of cells in the granule layer.

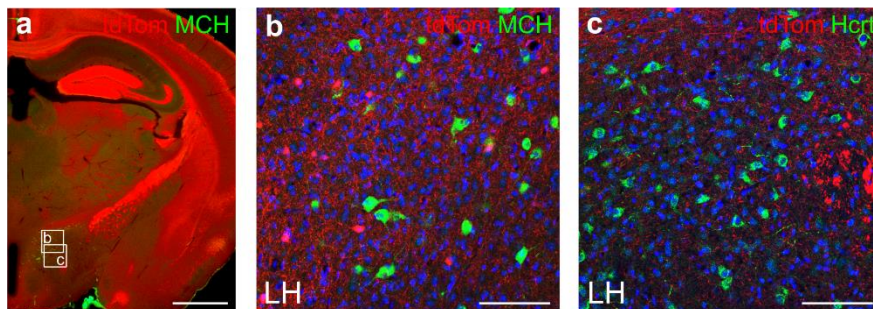
As evident from the boxed regions in (a,d), the tdTomato+ cells in different brain regions vary in their fluorescence intensity, therefore the images in panels (b,c,e) were acquired with settings optimised to show the tdTomato+ cells in each brain region.

CTX: neocortex. DAPI: 4',6-diamidino-2-phenylindole. DG: dentate gyrus. VLPO: ventrolateral preoptic hypothalamus. Scale bars: 1mm (a,d), 100 μ m (b,c,e)



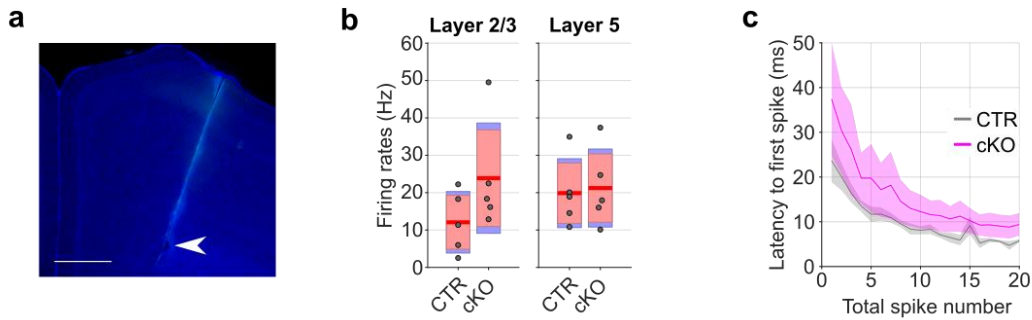
Suppl. Figure 4: The suprachiasmatic nucleus of the hypothalamus is void of Cre+ cells and spared of fibre tracts in the Rbp4-Cre driver line.

(a) Epifluorescence image of an Rbp4-Cre;Ai14;Snap25^{fl/+} brain section at the level of the suprachiasmatic nucleus (SCN). The section was counterstained with DAPI (blue). Box indicates approximate region from which image in (b) was taken. (b) High-magnification epifluorescence image of the SCN region. Rbp4-Cre;Ai14 axons are shown in red, cell nuclei stained with DAPI in blue. Note that there are no Cre+ cells located within the SCN (outlined with white dotted lines), and very few of the dense axon bundles pass through the SCN. DAPI: 4',6-diamidino-2-phenylindole. SCN: suprachiasmatic nucleus. Scale bars: 1mm (a), 100 μ m (b)



Suppl. Figure 5: No overlap between orexin or melanin concentrating hormone-expressing cells with Rbp4-Cre+ cells but dense fibre tracts in lateral hypothalamus.

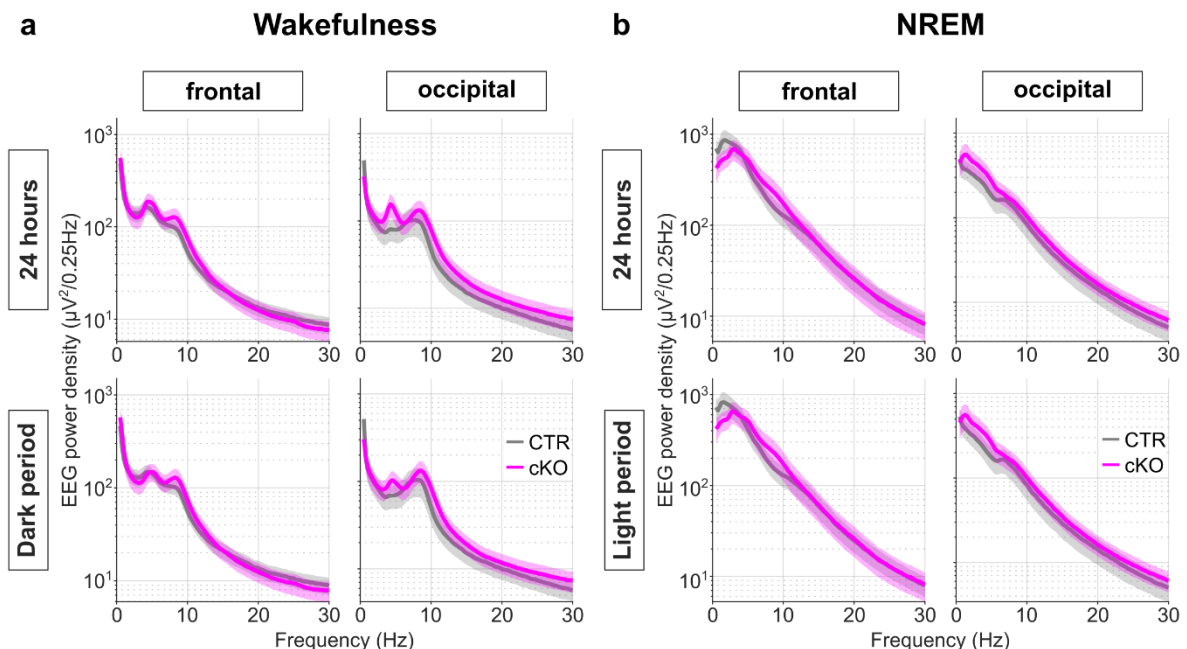
(a) Epifluorescence image of an Rbp4-Cre;Ai14;Snap25^{fl/+} brain hemisection at the level of the lateral hypothalamic area (LH), stained for melanin concentrating hormone (MCH) in green. Boxes indicate approximate regions from which images in (b,c) were taken. (b,c) Laser scanning confocal microscope images of two representative sections of LH of the same brain as shown in (a) stained for MCH (b) or orexin/hypocretin (Hcrt; c). Rbp4-Cre;Ai14 cells and processes are shown in red, and nuclei are counterstained with DAPI (blue). Note that no MCH+ cell was tdTom+ (n=3 brains, 692 MCH+ cells), and no Hcrt+ cell was tdTom+ (n=3 brains, 469 Hcrt+ cells). Note the dense fine fibres surrounding cell bodies in LH, consistent with an axonal terminal field in that region. DAPI: 4',6-diamidino-2-phenylindole. Hcrt: orexin/hypocretin. MCH: melanin concentrating hormone. tdTom: tdTomato. Scale bars: 1mm (a), 100 μ m (b,c)



Suppl. Figure 6: Laminar recordings from the transgenic mouse model show no significant genotype differences in laminar firing rates or latency to the first spike in layer 5.

a) Representative histology of a laminar implant in a cKO animal. The composite image shows fine electrode marks (green channel) and the DAPI counterstain of the coronal section (blue channel). An electrical microlesion (white arrow), performed under terminal anaesthesia to aid the histological assessment of the electrode depth, is visible at the level of the deepest channel of the laminar implant. b) Firing rates across neocortical layers 2/3 and 5 of both genotypes during non-rapid eye movement (NREM) sleep. c) Latency to the first spike at OFF-ON transitions in layer 5 of cKO and CTR animals. No significant genotype differences in the firing rates or in the latency to the first spike at any given spike number were found. Number of animals: n=5 CTR and n=5 cKO. Statistical methods and results provided in Suppl. Table 1.

cKO: conditional knockout animals. CTR: control animals. NREM: Non-rapid eye movement sleep. Scale bar histology image 500 μ m.



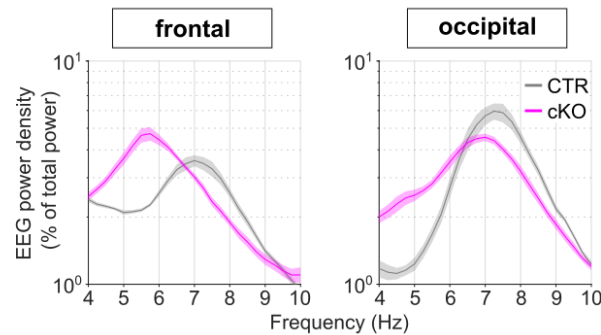
Suppl. Figure 7: EEG power spectra from the frontal and occipital derivations during waking and NREM sleep at baseline show no differences between genotypes.

a) Wake EEG power spectra over 24h and during the dark period, when mice are mostly awake. b) NREM EEG power spectra over 24h and during the light period, when mice are mostly asleep. No significant genotype differences in either derivation or condition were

found. Number of animals: n=5 CTR and n=8 cKO for EEG spectral analysis. Statistical methods and results provided in Suppl. Table 1.

cKO: conditional knockout animals. CTR: control animals. EEG: Electroencephalogram.

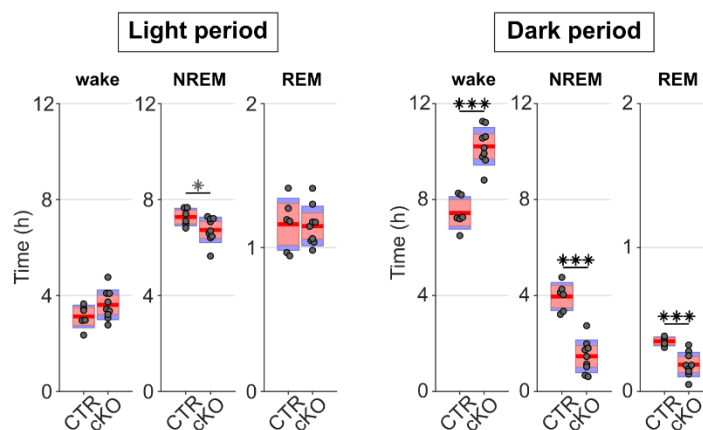
NREM: Non-rapid eye movement sleep.



Suppl. Figure 8: The theta peak during REM sleep is shifted towards lower frequencies in cortical SNAP25-ablated mice.

EEG spectral power in the frequency range between 4 and 10 Hz normalised to the mean spectral power over the entire EEG spectrum (0.5 – 30 Hz) during REM sleep on the baseline day. Note that the peak of theta activity is shifted towards lower frequencies in cKOs compared to CTRs in both the frontal and occipital EEG derivations. Number of animals: n=5 CTR and n=8 cKO for EEG spectral analysis. Statistical methods and results provided in Suppl. Table 1.

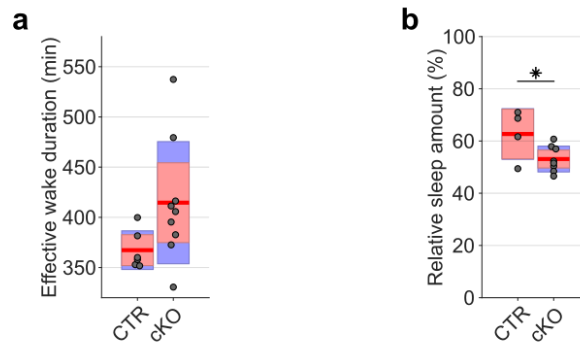
cKO: conditional knockout animals. CTR: control animals. EEG: Electroencephalogram. REM: Rapid eye movement sleep.



Suppl. Figure 9: Genotype differences in the amount of time spent in wake, NREM, and REM sleep during undisturbed baseline recordings are more pronounced in the dark period.

During the light period, the distribution between vigilance states is similar between genotypes with only a trend towards increased wakefulness and reduced NREM and REM sleep, while strong differences occur during the dark period. Black asterisks indicate post-hoc contrasts with significant differences ($*p < 0.05$, $**p < 0.01$, $***p < 0.001$), grey asterisks indicate post-hoc comparisons with $P < 0.05$, which do not reach significance after Bonferroni correction for multiple comparisons. Statistical methods and results provided in Suppl. Table 1. Data is presented as group mean (red line), 95% confidence interval (pink

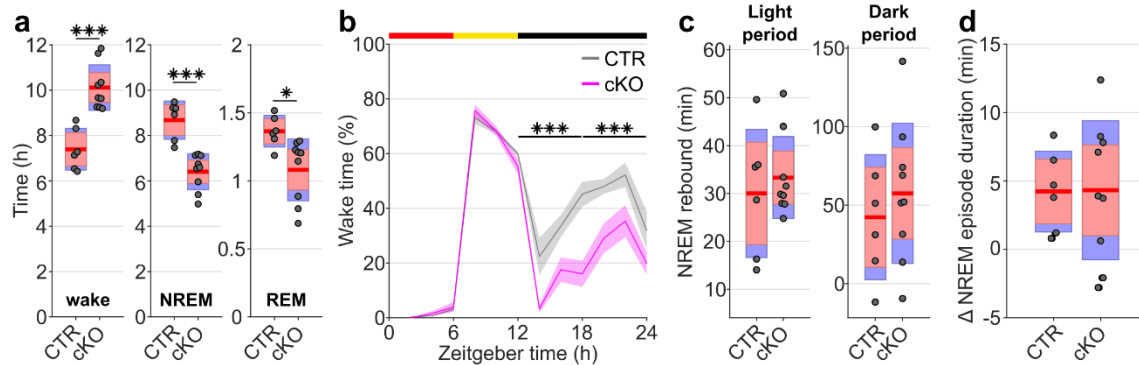
box), and one standard deviation (blue box) with individual data points overlaid. Number of animals: n=6 CTR and n=9 cKO for vigilance state analysis. cKO: conditional knockout animals. CTR: control animals. NREM: Non-rapid eye movement sleep. REM: Rapid eye movement sleep.



Suppl. Figure 10: Effective wake episode duration and circadian timing of the sleep deprivation experiment influence the amount of rebound sleep.

a) Effective wake duration (wake time during sleep deprivation plus wake bout duration preceding sleep deprivation) in a sleep deprivation experiment performed during the first half of the light period (Zeitgeber time 0-6). Assessment of the wake duration, based on EEG and EMG, shows a trend towards longer wake times in cortical SNAP25-ablated animals (cKO) compared to controls (CTR). Most cKO animals were already awake when sleep deprivation started while most CTR animals were asleep. b) Relative amount of sleep over 24 hours starting with the beginning of sleep deprivation compared to the preceding 24h interval in a sleep deprivation experiment performed during the second half of the light period (Zeitgeber time 6-12) under passive infrared recordings (PIR). Due to the shift of the sleep deprivation time window animals from both genotypes were able to sleep during the early light period before sleep deprivation started. Sleep deprivation during this time window results in a reduced relative amount of sleep in cortical SNAP25-ablated mice (cKO) compared to Cre-negative controls (CTR). Statistical methods and results provided in Suppl. Table 1. Data is presented as group mean (red line), 95% confidence interval (pink box), and one standard deviation (blue box) with individual data points overlaid. Number of animals: n=6 CTR and n=9 cKO for sleep deprivation experiment in EEG setup, n=4 CTR and n=8 cKO for sleep deprivation experiment in PIR setup.

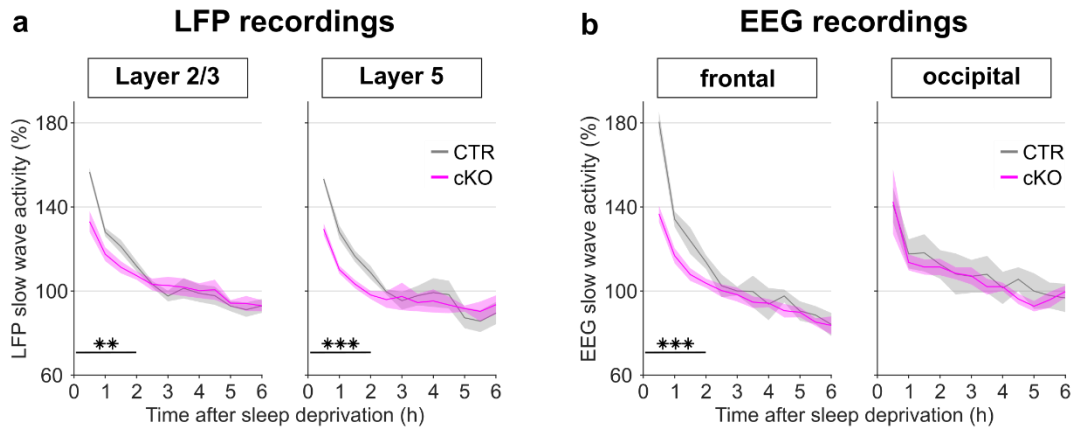
cKO: conditional knockout animals. CTR: control animals. EEG: Electroencephalogram.



Suppl. Figure 11: Absolute time in NREM sleep following sleep deprivation is reduced in cortical SNAP25-ablated animals but relative NREM rebound does not differ between genotypes.

a) Time spent in vigilance states (wake, NREM, and REM) during the 18 h recovery time following sleep deprivation. Note that overall cortical SNAP25-ablated animals (cKO) spent more time awake and less time in NREM and REM sleep compared to controls (CTR). b) Time course of NREM sleep on a sleep deprivation day compared between genotypes. Note that cKOs and CTRs do not differ in the time spent in NREM sleep during sleep deprivation (red bar above graph) or during the subsequent 6-h interval, but cKOs sleep less during the entire 12 h dark period following sleep deprivation. c) Rebound of NREM sleep time following sleep deprivation relative to individual baseline values. Note that both genotypes show a modest increase in the amount of NREM sleep relative to baseline after sleep deprivation during both the light and dark period with no differences between genotypes. d) Change in duration of NREM episodes during the first hour after sleep deprivation (ZT6-7 of SD day) relative to the same time window on BL day. Note that there is no difference in the initial increase of NREM episode duration between genotypes. Black asterisks indicate post-hoc contrasts with significant differences ($*p < 0.05$, $**p < 0.01$, $***p < 0.001$). Statistical methods and results provided in Suppl. Table 1. Data in panels a,c,d is presented as group mean (red line), 95% confidence interval (pink box), and one standard deviation (blue box) with individual data points overlaid. Number of animals: $n=6$ CTR and $n=9$ cKO for vigilance state analysis.

BL: baseline. cKO: conditional knockout animals. CTR: control animals. NREM: Non-rapid eye movement sleep. REM: Rapid eye movement sleep. SD: sleep deprivation. ZT: zeitgeber time.

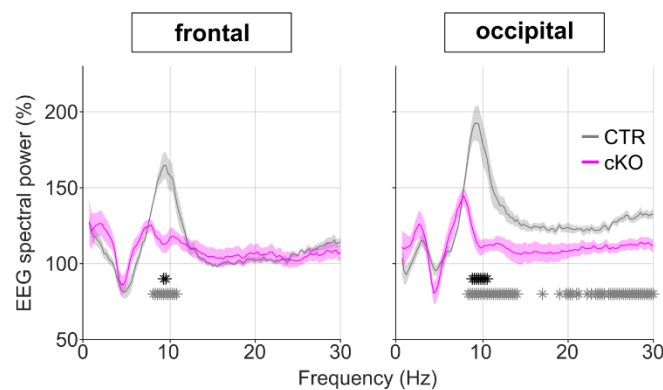


Suppl. Figure 12: The rebound of slow wave activity after sleep deprivation is specific to cortical areas but not layers.

Time course of NREM slow wave activity (SWA) after sleep deprivation (a) in the LFPs from layers 2/3 and 5 in primary motor cortex and (b) in the frontal and occipital EEG derivation. Note that cortical SNAP25-ablated animals (cKO) compared to controls (CTR) show a lower level of initial slow wave activity after sleep deprivation in the frontal cortex in the EEG and in LFPs from different cortical depths but not in the occipital EEG. Black asterisks indicate post-hoc contrasts with significant differences ($*p < 0.05$, $**p < 0.01$, $***p < 0.001$).

Statistical methods and results provided in Suppl. Table 1. Number of animals: $n=5$ CTR and $n=5$ cKO for laminar analysis, $n=5$ CTR and $n=8$ cKO for EEG spectral analysis.

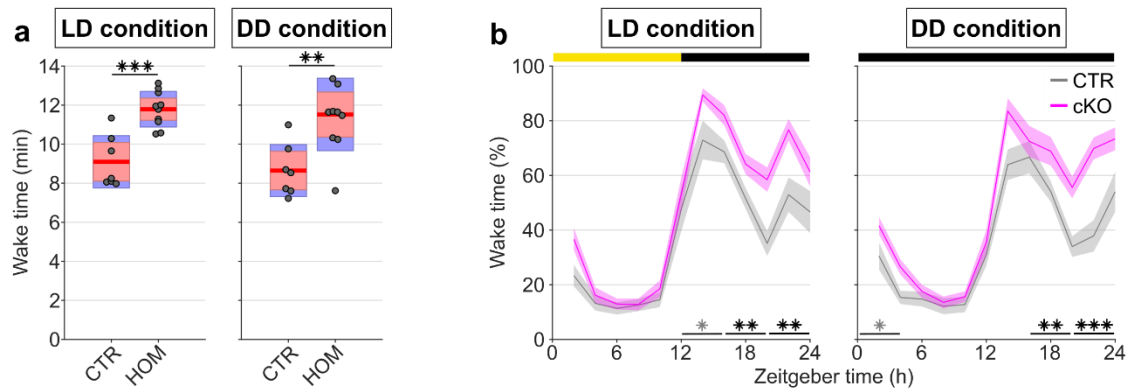
cKO: conditional knockout animals. CTR: control animals.



Suppl. Figure 13: Relative EEG power spectra during sleep deprivation show attenuation of theta increase in cortical SNAP25-ablated animals.

Wake EEG spectral power during the 6-hour sleep deprivation shown as a frequency bin-wise percentage of 24h baseline values. Note that the expected increase in the theta-power during sleep deprivation, which is visible in CTR mice, is severely diminished in cKOs.

Individual asterisks indicate spectral bins with significant differences in post-hoc comparison before (grey) and after (black) Bonferroni adjustment of α . Number of animals: $n=5$ CTR and $n=8$ cKO for EEG spectral analysis. Statistical methods and results provided in Suppl. Table 1. cKO: conditional knockout animals. CTR: control animals. EEG: electroencephalogram.



Suppl. Figure 14: Passive infrared recordings (PIR) show robustness of sleep phenotype to altered light-conditions.

a) Wake time estimates averaged over the last 3 days of PIR recordings under 12:12 light-dark (LD) conditions and over the first 3 days of constant darkness (DD). Note that the PIR data replicates the genotype differences in wake amount observed in the EEG study and that the genotype differences in the daily amount of wakefulness persist in the absence of light. b) Time course of wakefulness in LD and DD conditions. Note that the distribution of wakefulness over the 24 h day is maintained in the absence of light indicating that cortical SNAP25-ablated animals stay rhythmic, even in the absence of the main zeitgeber (i.e. light). Black asterisks indicate post-hoc contrasts with significant differences ($*p < 0.05$, $**p < 0.01$, $***p < 0.001$), grey asterisks indicate post-hoc comparisons with $P < 0.05$, which do not reach significance after Bonferroni correction for multiple comparisons. Statistical methods and results provided in Suppl. Table 1. Data in panel a is presented as group mean (red line), 95% confidence interval (pink box), and one standard deviation (blue box) with individual data points overlaid. Number of animals: $n=7$ CTR and $n=10$ for PIR recordings. cKO: conditional knockout animals. CTR: control animals. LD: light:dark. DD: constant darkness. PIR: passive infrared recordings.

Suppl. Table 1: A Summary of ANOVA Results*

* Significant 2-way interactions were followed up with Bonferroni-adjusted post hoc comparisons with $\alpha_{\text{corrected}} = 0.05/k$, where k represents the number of post hoc comparisons; however, Bonferroni correction was not applied to post hoc comparisons involving EEG spectral frequency bins and $\alpha_{\text{uncorrected}} = 0.05$ was adopted. For these spectral analyses we report frequency bins with significant differences in post-hoc comparison before ($\alpha_{\text{uncorrected}}$) and after Bonferroni adjustment of α ($\alpha_{\text{corrected}}$). All post hoc comparisons were conducted as 1-way ANOVAs involving 2 factor levels; in these cases, the F statistics is equivalent and can be converted to the t statistics by $t = \sqrt{F}$

Figure	Type of factorial ANOVA; number of post hoc comparisons (k)	Results
Fig. 1g	Genotype (CTR vs. cKO) \times Time (30 1-ms bins) ANOVA followed by 3 Bonferroni-adjusted post hoc comparisons of Genotype in 10-ms bins 1-way Genotype (CTR vs. cKO) ANOVA on time to peak	<ul style="list-style-type: none"> Genotype \times Time interaction $F(29,232) = 4.326$, $p < 0.001$, with CTR > cKO in the first 10 ms, $p = 0.009$ Longer surge time in cKO animals $F(1,8) = 10.081$, $p = 0.013$
Fig. 1h	Genotype (CTR vs. cKO) \times Cortical Layer (L2/3 vs. L5) ANOVA on slow-wave amplitude followed by 4 Bonferroni-adjusted post hoc comparisons, including simple effects of Genotype in L2/3 and L5 and simple effects of Cortical Layer in CTR and cKO 1-way Genotype (CTR vs. cKO) ANOVA on L5 to L2/3 slow wave amplitude ratio	<ul style="list-style-type: none"> Genotype \times Cortical Layer interaction $F(1,8) = 95.172$, $p < 0.001$. Post hoc comparisons by layer: <ul style="list-style-type: none"> CTR > cKO in L5, $p = 0.006$ cKO > CTR in L2/3, $p = 0.058$ Post hoc comparisons by genotype: <ul style="list-style-type: none"> L5 > L2/3 in CTR, $p < 0.001$ L5 > L2/3 in cKO, $p = 0.030$ Main effect of Genotype on slow wave amplitude ratio $F(1,8) = 10.835$, $p = 0.011$
Fig. 1i	Genotype (CTR vs. cKO) \times Cortical Layer (L2/3 vs. L5) ANOVA on laminar slow-wave activity followed by 4 Bonferroni-adjusted post hoc comparisons, including simple effects of Genotype in L2/3 and L5 and simple effects of Cortical Layer in CTR and cKO 1-way Genotype (CTR vs. cKO) ANOVA on L5 to L2/3 slow wave activity ratio Genotype (CTR vs. cKO) \times Cortical Layer (L2/3 vs. L5) \times Spectral Frequency (119 0.25-Hz bins) ANOVAs on LFP spectra NREM sleep followed by Cortical Layer \times Spectral Frequency ANOVAs for each genotype separately and uncorrected post hoc comparisons of Layers in 119 0.25-Hz bins	<ul style="list-style-type: none"> Genotype \times Cortical Layer interaction $F(1,8) = 114.820$, $p < 0.001$ Post hoc comparisons by layer: <ul style="list-style-type: none"> CTR > cKO in L5, $p = 0.021$ cKO > CTR in L2/3, $p = 0.015$ Post hoc comparisons by genotype: <ul style="list-style-type: none"> L5 > L2/3 in CTR, $p < 0.001$ L5 > L2/3 in cKO, $p = 0.385$ Main effect of Genotype on slow wave activity ratio $F(1,8) = 53.68$, $p < 0.001$ Genotype \times Cortical Layer \times Spectral Frequency interaction $F(118,944) = 24.842$, $p < 0.001$ Cortical Layer \times Spectral Frequency interaction, $F(118,472) = 87.078$, $p < 0.001$, L5 > L2/3 in frequency bins 1-32, $p < 0.05$ ($\alpha_{\text{uncorrected}}$), frequency bins 4-13 ($\alpha_{\text{corrected}}$), bin size 0.25 Hz with bin 1=0.5 Hz and bin 119=30 Hz Cortical Layer \times Spectral Frequency interaction, $F(118,472) = 11.753$, $p < 0.001$, L5 > L2/3 in frequency bins 6, 7, L2/3 > L5

		in frequency bins 14-119, $p_s < 0.05$ ($\alpha_{\text{uncorrected}}$), frequency bins 19-24 ($\alpha_{\text{corrected}}$), bin size 0.25 Hz with bin 1=0.5 Hz and bin 119=30 Hz
Fig. 1j	Genotype (CTR vs. cKO) \times Spectral Frequency (119 0.25-Hz bins) ANOVAs on frontal EEG spectra during wakefulness	<ul style="list-style-type: none"> Genotype \times Spectral Frequency interaction $F(118,1298) = 1.998$, $p < 0.001$, but no significant effect of Genotype in any of the 119 0.25-Hz bins, $p_s > 0.5$
	Genotype (CTR vs. cKO) \times Spectral Frequency (119 0.25-Hz bins) ANOVAs on frontal EEG spectra during NREM sleep	<ul style="list-style-type: none"> Genotype \times Spectral Frequency interaction $F(118,1298) = 2.793$, $p < 0.001$, but no significant effect of Genotype in any of the 119 0.25-Hz bins, $p_s > 0.2$
Fig. 2c	Genotype (CTR vs. cKO) \times Vigilance State (Wake, NREM, and REM) ANOVA followed by 3 Bonferroni-adjusted post hoc comparisons of Genotype under the three vigilance states	<ul style="list-style-type: none"> Genotype \times Vigilance State interaction Greenhouse-Geisser $F(1.056,13.732) = 33.008$, $p < 0.001$, with cKO > CTR in Wake state, $p < 0.001$, and CTR > cKO in NREM state, $p < 0.001$
Fig. 2d	Genotype (CTR vs. cKO) \times Time (12 2-h bins) ANOVA followed by 6 Bonferroni-adjusted post hoc comparisons of Genotype in 4-h bins	<ul style="list-style-type: none"> Main effect of Genotype $F(1,13) = 30.804$, $p < 0.001$ and Genotype \times Time interaction Greenhouse-Geisser $F(5,67) = 3.467$, $p = 0.007$, with cKO > CTR for the entire 12-h night, $p_s < 0.005$, cKO > CTR also approaching significance ($\alpha_{\text{corrected}}$: $p = 0.008$) from ZT0 h to ZT4 h, $p = 0.023$
Fig. 2e	Separate 1-way Genotype (CTR vs. cKO) ANOVAs on maximum and average wake duration	<ul style="list-style-type: none"> Main effect of Genotype on maximum wake duration $F(1,13) = 11.326$, $p = 0.005$ and main effect of Genotype on average wake duration $F(1,13) = 24.392$, $p < 0.001$
Fig. 2f	General linear model with 5 factors: MouseID, MouseID \times Episode Duration (random factors), Genotype, Episode Duration, and Genotype \times Episode Duration (fixed factors); dependent variable: SWA Ratio post/pre sleep;	<ul style="list-style-type: none"> Main effect of Genotype on SWA Ratio post/pre sleep $F(1,57.37) = 6.44$, $p = 0.014$
Fig. 3b	Genotype (CTR vs. cKO) \times Time (12 30-min bins) ANOVA followed by 3 Bonferroni-adjusted post hoc comparisons of Genotype in 2-h bins	<ul style="list-style-type: none"> Genotype \times Time interaction $F(11,121) = 7.561$, $p < 0.001$, with CTR > cKO in the first 2 h, $p < 0.001$
Fig. 3c	Genotype (CTR vs. cKO) \times Spectral Frequency (119 0.25-Hz bins) ANOVA followed by uncorrected post hoc comparisons of Genotype in 119 0.25-Hz bins	<ul style="list-style-type: none"> Genotype \times Spectral Frequency interaction $F(118,1298) = 4.068$, $p < 0.001$, due to CTR > cKO in frequency bins 2–14, 17–19, 32–36, 38, 42, 99–102, 107, and 110, $p_s < 0.05$ ($\alpha_{\text{uncorrected}}$), frequency bins 4-6, 9, 10 ($\alpha_{\text{corrected}}$), bin size 0.25 Hz with bin 1=0.5 Hz and bin 119=30 Hz
Figs. 3e and 3f	Genotype (CTR vs. cKO) multivariate ANOVA with 3 response variables, including period length (τ), periodogram power (Qp), and phase shift ($\Delta\phi$)	<ul style="list-style-type: none"> No main effect of Genotype, Wilks' λ $F(3,13) = 0.487$, $p = 0.697$; τ: $F(1,15) = 0.695$, $p = 0.418$; Qp: $F(1,15) = 0.304$, $p = 0.590$; and $\Delta\phi$: $F(1,15) = 0.399$, $p = 0.537$

Suppl. Fig. 1, <i>left</i>	Cortical Layer (L2/3 vs. L5) × Time (30 1-ms bins) ANOVA followed by 3 Bonferroni-adjusted post hoc comparisons of Cortical Layer in 10-ms bins	<ul style="list-style-type: none"> Cortical Layer × Time interaction $F(29,174) = 9.412$, $p < 0.001$, with L5 > L2/3 in the first 10 ms, $p = 0.008$
Suppl. Fig. 1, <i>right</i>	Cortical Layer (L2/3 vs. L5) × Count (20 1-spike bins) ANOVA followed by 10 Bonferroni-adjusted post hoc comparisons of Cortical Layer in 2-spike bins	<ul style="list-style-type: none"> Main effect of Cortical Layer $F(1,6) = 86.301$, $p < 0.001$ and Cortical Layer × Count interaction $F(17,102) = 27.205$, $p < 0.001$, with L5 < L2/3 in all spike count bins, $ps < 0.001$
Suppl. Fig. 6b	Genotype (CTR vs. cKO) × Layer (L2/3 vs. L5) ANOVA followed by 2 Bonferroni-adjusted post hoc comparisons of Genotype for the two layers	<ul style="list-style-type: none"> No Genotype × Layer interaction $F(1,8) = 0.946$, $p = 0.359$, no significant effect of Genotype in any of the layers, $ps > 0.1$
Suppl. Fig. 6c	Genotype (CTR vs. cKO) × Count (16 1-spike bins) ANOVA followed by 16 Bonferroni-adjusted post hoc comparisons of Genotype. Note: spike counts 17-20 were excluded from the ANOVA due to insufficient data in one CTR animal	<ul style="list-style-type: none"> No Genotype × Count interaction $F(15,120) = 0.750$, $p = 0.730$, no significant effect of Genotype in any of the spike count bins, $ps > 0.1$
Suppl. Fig. 7a	Genotype (CTR vs. cKO) × Spectral Frequency (119 0.25-Hz bins) ANOVAs on frontal and occipital wake EEG spectra during baseline	<ul style="list-style-type: none"> For frontal and occipital EEG spectra during the 24-h period, Genotype × Spectral Frequency interactions $F(118,1298) = 1.998$, $p < 0.001$ and $F(118,1298) = 2.730$, $p < 0.001$, but no significant effect of Genotype in any of the 119 0.25-Hz bins, $ps > 0.05$ For frontal and occipital EEG spectra during the dark period, Genotype × Spectral Frequency interactions $F(118,1298) = 1.614$, $p < 0.001$ and $F(118,1298) = 1.905$, $p < 0.001$, but no significant effect of Genotype in any of the 119 0.25-Hz bins, $ps > 0.05$
Suppl. Fig. 7b	Genotype (CTR vs. cKO) × Spectral Frequency (119 0.25-Hz bins) ANOVAs on frontal and occipital NREM EEG spectra during baseline	<ul style="list-style-type: none"> For frontal EEG spectra during the 24-h period, Genotype × Spectral Frequency interaction $F(118,1298) = 2.793$, $p < 0.001$, but no significant simple effect of Genotype in any of the 119 0.25-Hz bins, $ps > 0.05$ For occipital EEG spectra during the 24-h period, no significant main effect of Genotype or Genotype × Spectral Frequency interaction, $p > 0.7$ For frontal EEG spectra during the light period, Genotype × Spectral Frequency interaction $F(118,1298) = 2.693$, $p < 0.001$, but no significant simple effect of Genotype in any of the 119 0.25-Hz bins, $ps > 0.05$ For occipital EEG spectra during the light period, no significant main effect of Genotype or Genotype × Spectral Frequency interaction $F(118,1298) = 1.193$, $p = 0.086$, no significant simple effect of

			Genotype in any of the 119 0.25-Hz bins, $p_s > 0.05$
Suppl. Fig. 8		Genotype (CTR vs. cKO) × EEG Derivation (Frontal vs. Occipital) ANOVA on peak theta frequency followed by 2 post hoc comparisons of Genotype for frontal and occipital EEG	<ul style="list-style-type: none"> Main effect of Genotype $F(1,11) = 33.532$, $p < 0.001$ and Genotype × EEG Derivation interaction $F(1,11) = 14.233$, $p = 0.003$ CTR > cKO for both frontal and occipital EEG-derived peak theta frequency, $p < 0.001$ and $p = 0.01$, respectively
Suppl. Fig. 9		Genotype (CTR vs. cKO) × Phase (Light vs. Dark) × Vigilance State (Wake, NREM, and REM) ANOVA, followed by Genotype (CTR vs. cKO) × Phase (Day vs. Night) ANOVAs for each vigilance state and 6 Bonferroni-adjusted post hoc comparisons of Genotype	<ul style="list-style-type: none"> 3-way Genotype × Phase × Vigilance State interaction Greenhouse-Geisser $F(1,14) = 36.083$, $p < 0.001$ For Wake state, Genotype × Phase interaction $F(1,13) = 36.961$, $p < 0.001$, with cKO > CTR at night, $p < 0.001$ For NREM state, Genotype × Phase interaction $F(1,13) = 36.352$, $p < 0.001$, with CTR > cKO at night, $p < 0.001$, CTR > cKO approaching significance at day ($\alpha_{\text{corrected}}: p = 0.008$), $p = 0.049$ For REM state, Genotype × Phase interaction approached significance, $F(1,13) = 3.703$, $p = 0.076$, with CTR > cKO at night, $p = 0.001$
Suppl. 10a	Fig.	1-way Genotype (CTR vs. cKO) ANOVA on effective wake duration	<ul style="list-style-type: none"> Main effect of Genotype on effective wake duration approached significance, $F(1,13) = 3.325$, $p = 0.091$
Suppl. 10b	Fig.	1-way Genotype (CTR vs. cKO) ANOVA on relative sleep amount	<ul style="list-style-type: none"> Main effect of Genotype on relative sleep amount, $F(1,10) = 5.405$, $p = 0.042$
Suppl. 11a	Fig.	Genotype (CTR vs. cKO) × Vigilance State (Wake, NREM, and REM) ANOVA followed by 3 Bonferroni-adjusted post hoc comparisons of Genotype under the three vigilance states	<ul style="list-style-type: none"> Genotype × Vigilance State interaction Greenhouse-Geisser $F(1,14) = 27.754$, $p < 0.001$, with cKO > CTR in Wake state, $p < 0.001$, CTR > cKO in NREM state, $p < 0.001$, and CTR > cKO in REM state, $p = 0.015$
Suppl. 11b	Fig.	Genotype (CTR vs. cKO) × Time (12 2-h bins) ANOVA followed by 4 Bonferroni-adjusted post hoc comparisons of Genotype in 6-h bins	<ul style="list-style-type: none"> Main effect of Genotype $F(1,13) = 25.540$, $p < 0.001$ and Genotype × Time interaction Greenhouse-Geisser $F(4,54) = 4.222$, $p = 0.004$, with cKO > CTR for the entire 12-h night, $p_s \leq 0.001$
Suppl. 11c	Fig.	Genotype (CTR vs. cKO) × Phase (Light vs. Dark) ANOVA on NREM rebound after sleep deprivation	<ul style="list-style-type: none"> No significant effects. No Genotype × Phase interaction $F(1,13) = 0.253$, $p = 0.623$. No effect of Genotype $F(1,13) = 0.657$, $p = 0.432$.
Suppl. 11d	Fig.	1-way Genotype (CTR vs. cKO) ANOVA on change in NREM episode duration	<ul style="list-style-type: none"> No significant effect, $F(1,13) = 0.002$, $p = 0.967$
Suppl. Fig. 12		Genotype (CTR vs. cKO) × Spectral Frequency (119 0.25-Hz bins) ANOVAs on frontal and occipital wake EEG spectra during sleep	<ul style="list-style-type: none"> For frontal wake EEG spectrum, Genotype × Spectral Frequency interaction $F(118,1298) = 5.807$, $p < 0.001$, due to CTR > cKO in frequency bins 31–42, $p_s < 0.05$

		deprivation, followed by uncorrected post hoc comparisons of Genotype in 119 0.25-Hz bins	<p>($\alpha_{\text{uncorrected}}$), frequency bins 36, 37 ($\alpha_{\text{corrected}}$), bin size 0.25 Hz with bin 1=0.5 Hz and bin 119=30 Hz</p> <ul style="list-style-type: none"> For occipital wake EEG spectrum, Genotype \times Spectral Frequency interaction $F(118,1298) = 10.007$, $p < 0.001$, due to CTR > cKO in frequency bins 31–55, 67, 75, 78–81, 83–84, 88, 90, 92–96, and 98–119, $p_s < 0.05$ ($\alpha_{\text{uncorrected}}$), frequency bins 34–41 ($\alpha_{\text{corrected}}$), bin size 0.25 Hz with bin 1=0.5 Hz and bin 119=30 Hz
Suppl. 13a	Fig.	Genotype (CTR vs. cKO) \times Cortical Layer (L2/3 vs. L5) \times Time (12 30-min bins) ANOVA, followed by Genotype (CTR vs. cKO) \times Time (3 2-h bins) ANOVAs for L2/3 and L5 and 6 Bonferroni-adjusted post hoc comparisons of Genotype in 2-h bins	<ul style="list-style-type: none"> 3-way Genotype \times Cortical Layer \times Time interaction approached significance, $F(11,88) = 1.803$, $p = 0.065$ For L2/3, Genotype \times Time interaction $F(2,16) = 8.699$, $p = 0.003$, with CTR > cKO in first 2 h, $p = 0.006$ For L5, Genotype \times Time interaction $F(2,16) = 9.022$, $p = 0.002$, with CTR > cKO in first 2 h, $p < 0.001$
Suppl. 13b	Fig.	Genotype (CTR vs. cKO) \times EEG Derivation (Frontal vs. Occipital) \times Time (12 30-min bins) ANOVA, followed by Genotype (CTR vs. cKO) \times Time (3 2-h bins) ANOVAs for frontal and occipital EEG and 6 Bonferroni-adjusted post hoc comparisons of Genotype in 2-h bins	<ul style="list-style-type: none"> 3-way Genotype \times EEG Derivation \times Time interaction approached significance, Greenhouse-Geisser $F(1.710,18.805) = 3.262$, $p = 0.067$ For frontal EEG, Genotype \times Time interaction $F(2,22) = 20.030$, $p < 0.001$, with CTR > cKO in first 2 h, $p < 0.001$ For occipital EEG, no Genotype \times Time interaction Greenhouse-Geisser $F(1.234,13.574) = 0.078$, $p = 0.835$, no significant effect involving Genotype, $p_s > 0.4$
Suppl. 14a	Fig.	Genotype (CTR vs. cKO) \times Lighting (LD vs. DD) ANOVA, followed by 2 Bonferroni-adjusted post hoc comparisons of Genotype under the two Lightning conditions	<ul style="list-style-type: none"> Main effect of Genotype $F(1,15) = 18.604$, $p = 0.001$, no interaction Lightning \times Genotype $F(1,15) = 0.116$, $p = 0.738$, cKO > CTR in LD condition $p < 0.001$ and DD condition $p = 0.003$
Suppl. 14b	Fig.	Genotype (CTR vs. cKO) \times Lighting (LD vs. DD) \times Time (12 2-h bins) ANOVA, followed by Genotype (CTR vs. cKO) \times Time (6 4-h bins) ANOVAs for each lighting condition and 12 Bonferroni-adjusted post hoc comparisons of Genotype in 4-h bins	<ul style="list-style-type: none"> Genotype \times Time interaction Greenhouse-Geisser $F(3.801,57.016) = 3.319$, $p = 0.018$ in LD condition cKO > CTR from ZT16h to ZT24 ($p_s < 0.01$) and approaching significance from ZT0 h to ZT4 h ($p = 0.072$) and ZT4 h to ZT8 h ($p = 0.011$) in DD condition cKO > CTR from ZT16h to ZT24 ($p_s < 0.01$) and approaching significance from ZT0 h to ZT4 h ($p = 0.012$)